Accounts

Photo- and Mechano-Catalytic Overall Water Splitting Reactions to Form Hydrogen and Oxygen on Heterogeneous Catalysts

Kazunari Domen,*,# Junko N. Kondo, Michikazu Hara, and Tsuyoshi Takata

Research Laboratory of Resources Utilization, Tokyo Institute of Technology, 4259 Nagatsuta, Midori-ku, Yokohama 226-8503

(Received December 27, 1999)

Recent progress of overall water splitting by photocatalysts and mechanocatalysts is briefly reviewed. In photocatalytic reactions, several new materials have been introduced, and the catalyst preparation has also been improved. As a result, a high quantum efficiency for overall water splitting of about 30% has been accomplished. In addition, recent progress in the understanding of the reaction mechanism is briefly introduced.

On the other hand, mechano-catalytic overall water splitting reaction has been recently discovered by the authors. The phenomenological aspects of this novel reaction are summarized, and some implications of the reaction mechanism are also described.

In the beginning of the 21st century, we will face serious global problems concerning energy and environment. Probably one of the most ideal and attractive solutions to those problems is the utilization of H_2 as a recyclable energy carrier on a huge scale. However, if H_2 is produced from fossil resources such as natural gas and petroleum, the H_2 production is inevitably accompanied by the formation of CO_2. Therefore, if human beings desire to obtain the ultimately clean H_2 as an energy resource, water is the only source of H_2 on the earth.[1]

The overall water splitting reaction to produce H_2 and O_2 is accompanied by a large increase of free energy, as shown in Eq. 1:

$$H_2O \rightarrow H_2 + 1/2O_2 \quad \Delta G^\circ = 238\ \mathrm{kJ\,mol^{-1}} \qquad (1)$$

To promote this reaction, some free energy sources other than thermal energy have to be injected. The energy diagram for such a reaction is depicted in Fig. 1. In photocatalysis and mechanocatalysis, such energies as are utilized for water decomposition are provided through so-called mediator photocatalysts and mechanocatalysts. The electronic states of these mediators are at first excited by photons or probably by mechanical energy. The important and difficult step is the subsequent energy transfer from the excited mediators to water molecules to generate H_2 and O_2 molecules. To facilitate the process, various kinds of modification have been attempted for photocatalysts. Another important condition for the effective overall water splitting is the prevention of the reverse reaction from the products. If the reaction system contains materials that work as effective catalysts for H_2O formation from H_2 and O_2, one can not expect to accumulate the product, H_2 and O_2, in the system.

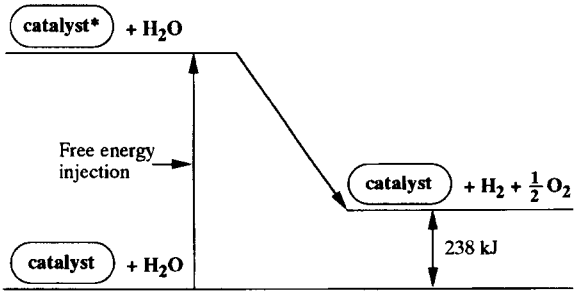

Fig. 1. The energy diagram for a free-energy injected overall water decomposition over a catalyst.

1. Photocatalytic Overall Water Splitting

1.1. Structures and Proposed Reaction Mechanisms of Some Typical Photocatalysts. The authors have reported several catalytic systems for overall water splitting. Three of them are schematically depicted in Fig. 2. All of these photocatalytic systems evolve H_2 and O_2 in the stoichiometric ratio under the steady state reaction condition. The optimized quantum efficiencies are about 1%, 10%, and 30% for systems (a), (b), and (c), respectively.

1.1(a). $SrTiO_3$.[2,3] In Fig. 2(a), nickel is loaded on $SrTiO_3$

CREST, JST (Japan Science and Technology).

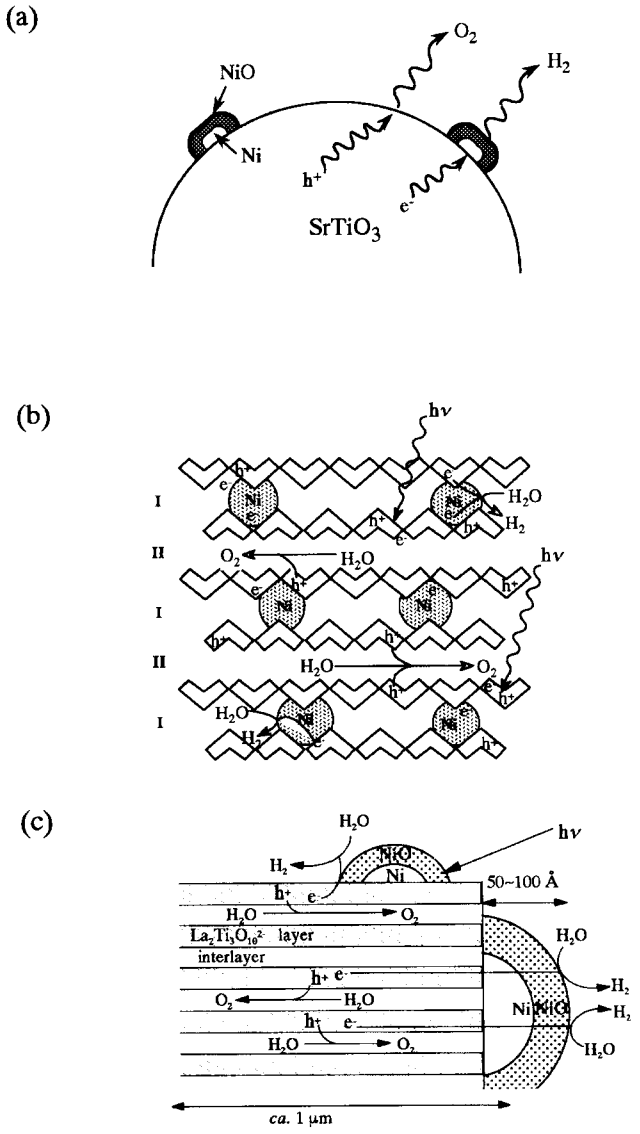

Fig. 2. Photocatalytic systems for overall water decomposition; (a) $NiO/SrTiO_3$, (b) $NiO/K_4Nb_6O_{17}$, and (c) $K_2La_2Ti_3O_{10}$. "Ni", "Ni/NiO" or "NiO" in figures corresponds to NiO after R773–O473 pretreatment.

as a catalyst to facilitate H_2 evolution. The Ni-loaded catalyst is prepared by impregnation in an aqueous $Ni(NO_3)_2$ solution, and is treated under proper conditions, i.e., H_2 reduction at 773 K for 2 h followed by reoxidation in O_2 at 473 K for 1 h (referred to as R773–O473). The inner sphere of the loaded NiO is reduced to Ni metal after H_2 reduction, and successive re-oxidation under a mild condition only oxidizes the external surface of Ni metal particles. All the nickel-loaded catalysts in following sections after R773–O473 treatment is referred to as NiO/Ni-catalysts below except $K_4Nb_6O_{17}$. The particle size of the loaded NiO is a few tens of nm, while $SrTiO_3$ consists of particles of a few μm in size. This structure is essential for the bulk type titanate- or niobate-based catalysts but it is not the case for tantalate-based ones (see Section 1.3.). If Ni metal is exposed to water at the external surface, only a small amount of H_2 is evolved under the band gap irradiation because Ni^{2+} is eluted by oxidation of Ni. The reverse reaction also proceeds on the remaining Ni particles.

1.1(b). $K_4Nb_6O_{17}$.[4] Figure 2(b) shows a photocatalytic system with an ion-exchangeable layered compound. The $K_4Nb_6O_{17}$ material consists of macropolyanion sheets of niobates ($Nb_6O_{17}^{4-}$); K^+ ions locate at the interlayer space. A noticeable feature of the niobate is that two different types of the interlayer spaces exist alternately[5] as is schematically depicted in the figure. Furthermore, the niobate sheet itself has anisotropy along the stacking direction, i.e. the sheet has a front and a back side. The interlayer spaces are hydrated in an aqueous solution. This indicates that the reactant, H_2O molecules, are easily intercalated into the interlayer space during the photocatalytic reaction. The two types of interlayer space exhibit different ion-exchange properties. K^+ ions at the interlayer space I are exchangeable by Li^+, Na^+, and some polyvalent cations such as Ni^{2+} while those at the interlayer space II are replaced only by monovalent cations.[5] This unique property results in a significant consequence as explained below.

$K_4Nb_6O_{17}$ alone in distilled water evolves H_2 and O_2 under the band gap (ca. 3.3 eV) irradiation, although the activity is low. A marked enhancement in activity of H_2O decomposition is observed when the catalyst is modified by nickel. The modification by RuO_2 or Pt was also effective to increase the activity under proper pretreatment conditions. The highest activity was obtained over Ni(0.1 wt%)–$K_4Nb_6O_{17}$ with R773–O473. A similar result was obtained for $Rb_4Nb_6O_{17}$, in which a higher quantum efficiency (ca. 10% at 330 nm) than that of $K_4Nb_6O_{17}$ (ca. 5% at 330 nm) was obtained.

From the structural studies by means of XPS (X-ray photoelectron spectroscopy), TEM (transmission electron microscopy) and EXAFS (extended X-ray absorption fine structure), the structure of active Ni(0.1 wt%)–$K_4Nb_6O_{17}$ catalyst was elucidated as shown in Fig. 2(b). Most of the loaded nickel is located in the interlayer I as metallic ultrafine particles (ca. 5 Å) after the R773–O473 treatment. It should be mentioned that the ultrafine nickel particles in the interlayer I are not oxidized by O473 treatment. This exclusive location of nickel metal particles was based on the work of Kinomura et al.[5] as mentioned above. On the basis of the structure of active Ni–$K_4Nb_6O_{17}$ catalyst, reaction mechanism of H_2O decomposition is also proposed as follows. The active sites for H_2 evolution are on the nickel metal ultrafine particles at the interlayer space I, and the active sites for O_2 evolution are in the interlayer space II. Therefore, active sites for H_2 and O_2 evolution are separated by each niobate sheet, which allows relatively high quantum efficiency (ca. 10% for $Rb_4Nb_6O_{17}$). Nevertheless, about 90% of the photoexcited electrons and holes do not follow the scenario, and the Ni metal particles are gradually oxidized by the holes and/or OH radicals to cause degradation of the activity.

1.1(c). $A_2La_2Ti_3O_{10}$ (A = K, Rb) and $A_{2-x}La_2Ti_{3-x}Nb_xO_{10}$ (x = 0.5 and 1.0).[6,7] Figure 2(c) shows another type of layered photocatalyst with a perovskite structure. The detailed structure of $A_2La_2Ti_3O_{10}$ (A = K, Rb) is depicted in

Fig. 3. Some partial substitutions of the Ti site by Nb are also possible to form $A_{2-x}La_2Ti_{3-x}Nb_xO_{10}$ ($x = 0.5$ and 1.0). One of the characteristics of $A_2La_2Ti_3O_{10}$ is the spontaneous hydration of its interlayer space. All of these perovskites were prepared by a conventional ceramic method, and the BET (Brunauer–Emmett–Teller) surface areas for these catalysts were about 1 $m^2 g^{-1}$. The same materials are also prepared by another preparation method which will be introduced in the following section. Band gaps estimated from UV-vis diffuse reflectance spectra are 3.4—3.5 eV for these perovskites.

The number of hydration and the optimum activity as well as the conditions (amount of loaded nickel and pH value of the solution) for each catalyst are summarized in Table 1. $Rb_2La_2Ti_3O_{10}$ with 4.0 wt% of Ni-loading in aqueous RbOH solution (0.1 M, pH = 12.8) showed the highest activity among the catalysts examined. The pretreatment of R773–O473 is also indispensable to evolve H_2 and O_2 steadily and efficiently. As shown in Table 1, the activity of $ALa_2Ti_2NbO_{10}$ catalysts ($x = 1.0$) is lower by about an order of magnitude than that of the others ($x = 0$, 0.5), while there is no evident difference in reaction behavior between $A_2La_2Ti_3O_{10}$ ($x = 0$) and $A_{1.5}La_2Ti_{2.5}Nb_{0.5}O_{10}$ ($x = 0.5$) catalysts. Although the interlayer space was not hydrated when one-third of Ti^{4+} was replaced by Nb^{5+}, i.e. $x = 1.0$, hydration took place for $A_2La_2Ti_3O_{10}$ and $A_{1.5}La_2Ti_{2.5}Nb_{0.5}O_{10}$ as seen from Table 1. Therefore, the lower activity of $ALa_2Ti_2NbO_{10}$ catalyst is due to the absence of hydration. The absence of hydration in the case of $ALa_2Ti_2NbO_{10}$ can be attributed to the relative amount of the alkaline metal cations at the interlayer space. These results indicate that the hydration of the interlayer space is essential to obtain high activity. From XPS and TEM, it was found that loaded nickel dominantly exists at the external surface, as in the case of Fig. 2(c). The particle size of nickel is 10—20 nm, and the inner sphere of each particle is metallic Ni and the outer sphere is NiO. According to the proposed reaction mechanism (Fig. 2(c)), H_2 evolution takes place on the NiO/Ni at the external surface, and O_2 evolution occurs at the interlayer space. Therefore, the reduction and oxidation sites of water are well enough separated to promote overall water splitting efficiently.

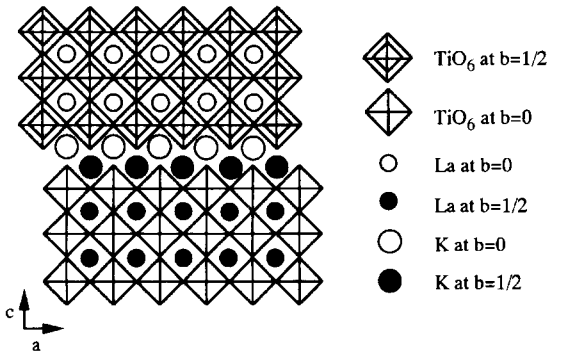

Fig. 3. Schematic structure of $K_2La_2Ti_3O_{10}$.

1.2. Effect of the Particle Size for Photocatalytic Decomposition of Water. In the above section, the structures and the proposed reaction mechanisms for two different types of layered photocatalysts are briefly introduced (Figs. 2(a), 2(b), and 2(c)). If the reaction mechanisms are strictly correct, the particle sizes of the layered oxides would not affect the quantum efficiency based on the number of the absorbed photons. To study this point in more detail, we attempted to prepare smaller-sized layered photocatalysts and we compared the activities with those previously reported.

1.2(a). Ni-Loaded $K_4Nb_6O_{17}$.[8] We were motivated to examine the effect of particle size on the catalytic activity by following experimental findings. The absorption coefficient of $K_4Nb_6O_{17}$ increases sharply from 360 nm to shorter wavelengths. The quantum efficiency for overall water splitting on Ni-loaded $K_4Nb_6O_{17}$ strongly depends upon the wavelength of irradiated light above the band-gap; the shorter the wavelength of the irradiated light is, the higher the quantum efficiency becomes.[9,10] We, therefore, considered that the irradiated light with shorter wavelength is almost absorbed near the external surface to cause decomposition of water into H_2 and O_2, while light with longer wavelength above the band-gap penetrates into the inner part of the particle,

Table 1. Photocatalytic Activities of Various Layered Perovskites and Hydration Numbers

Catalyst	Rate of gas evolution / μmol h^{-1}		Optimum condition			Hydration number
			NiO/Ni-loading	AOH		
	H_2	O_2	wt %[a]	mol dm^{-3}[b]	pH	n[c]
$K_2La_2Ti_3O_{10}$	444	221	3	0.1	12.8	1.0
$Rb_2La_2Ti_3O_{10}$	869	430	4	0.1	12.8	1.1
$Rb_{1.5}La_2Ti_{2.5}Nb_{0.5}O_{10}$	725	358	5	0.1	12.6	0.9
$RbLa_2Ti_2NbO_{10}$	79	30	0.3	0.1	12.8	0
$Cs_2La_2Ti_3O_{10}$	700	340	3	0	10.5	3.5
$Cs_{1.5}La_2Ti_{2.5}Nb_{0.5}O_{10}$	540	265	4	0	10.4	2.0
$CsLa_2Ti_2NbO_{10}$	115	50	0.3	0	8.5	0

a) Amount of loaded Ni. b) Concentration of aqueous AOH (A = K, Rb, Cs) solution. c) The number of hydration in the formula of $A_{2-x}La_2Ti_{3-x}Nb_xO_{10}\cdot nH_2O$.
Reaction condition; catalyst 1.0 g: H_2O 320 ml: high pressure mercury lamp (450 W): an inner irradiation type quartz reaction cell.

which may be less effective for the reaction. In other words, the interlayer space near the external surface may be more useful for the photodecomposition of water. From the above consideration, we attempted to prepare smaller $K_4Nb_6O_{17}$ particles which have higher external surface area by so-called ball milling method.

The original $K_4Nb_6O_{17}$ was prepared from a stoichiometric mixture of K_2CO_3 and Nb_2O_5 in a platinum crucible at 1473 K in air. The melted mixture was cooled down rapidly to room temperature and was pulverized in a mortar to form the powder with particle size of 1—10 μm. Millings were carried out by the following two methods. One was that suspension of $K_4Nb_6O_{17}$ (20 g) in 0.1 M KOH solution (1 M = 1 mol dm^{-3}) was put into a stainless vessel with zirconia beads and vigorously stirred by a feathered stirring rod made of Hastelloy for 1 h at room temperature. KOH was added to compensate for the elution of potassium ions from the interlayer as much as possible. The other method was that the suspension of $K_4Nb_6O_{17}$ (10 g) in distilled water was put into a centrifugal planetary ball mill (Fritsch) with zirconia beads and vigorously stirred for 2 h at room temperature. After both millings, the slurries were filtered to remove zirconia beads, then washed with water, centrifuged and dried in air at room temperature. The milled sample prepared by the former method is referred to as the milled (A) and the latter the milled (B).

Figure 4 shows the XRD (X-ray diffraction) patterns of an original powder of $K_4Nb_6O_{17}$ (Fig. 4(a)), the milled (A) (Fig. 4(b)), the milled (A) calcined at 773 K for 6 h (Fig. 4(c)), and the milled (B) (Fig. 4(d)). The original $K_4Nb_6O_{17}$ shows very strong peaks of *(0b0)* diffraction at lower angles. The structure is assigned to the hydrated form, $K_4Nb_6O_{17}\cdot 3H_2O$.[5]

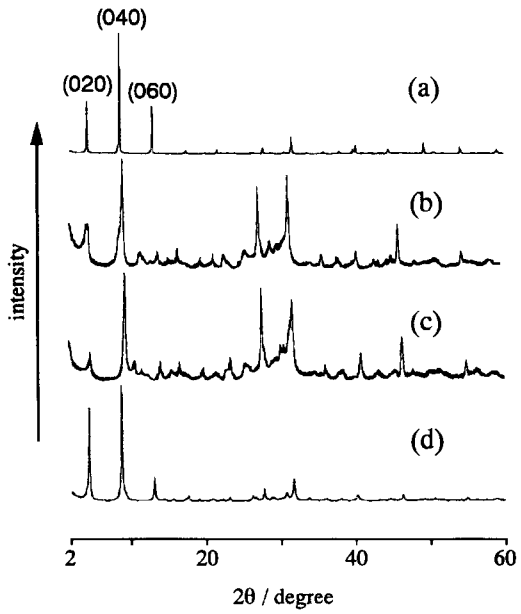

Fig. 4. XRD patterns of various $K_4Nb_6O_{17}$; a) original $K_4Nb_6O_{17}$ (pulverized in a mortar), b) milled (A) dried at r.t., c) the milled (A) calcined at 773 K, d) the milled (B) dried at r.t.

The milled (A) showed much weaker and broader peaks at the same positions than those of the original. These peaks slightly sharpened after calcination in air (Fig. 4(c)) but were not completely restored. Therefore, the crystal structure of the sample was found to be broken to some extent during the ball-milling treatment. On the other hand, the milled (B) maintained the crystal structure of the original $K_4Nb_6O_{17}$ very well. SEM observation showed that both the milled (A) and the (B) consisted of particles of 1—2 μm in diameter and much smaller (ca. 0.1 μm) ones, while most particles of the original $K_4Nb_6O_{17}$ were about 10 μm in diameter. BET surface area was measured by N_2 adsorption at 77 K. The surface areas after drying the samples were 17.3 and 11.2 $m^2 g^{-1}$ for the milled (A) and (B), respectively, while that of the original $K_4Nb_6O_{17}$ powder which was only pulverized in a mortar was smaller than 1 $m^2 g^{-1}$. When the milled samples were then calcined at various temperatures, the surface area decreased with increasing the calcination temperature and became 11.3 and 6.2 $m^2 g^{-1}$ for (A) and (B), respectively after calcination at 873 K.

Table 2 compares the photocatalytic activity for H_2 and O_2 evolution over Ni (0.1 wt%) and Ni (1.0 wt%)-loaded $K_4Nb_6O_{17}$ of the original, the milled (A) and the milled (B). In the case of Ni (0.1 wt%) loading, the activities of the milled (A) and (B) which were dried at room temperature were smaller than that of the original. However, when the milled catalysts were calcined before Ni loading, the pho-

Table 2. Rate of H_2 and O_2 Evolution from Water and BET Surface Areas of Various $K_4Nb_6O_{17}$ Powders

Catalyst	Amount of loading Ni (wt%)				BET
	0.1		1.0		
	Rate of gas evolution (μmol h^{-1})				surface area
	H_2	O_2	H_2	O_2	$m^2 g^{-1}$
Pulverized in a mortar (original)	774	370	784	394	<1
Ball-milling (A)					
Dried in air	578	248	1203	597	17.3
Calcination at 673 K	606	289	1316	653	14.6
Calcination at 773 K	906	483	1608	789	13.9
Calcination at 873 K	736	386	1466	734	11.3
Ball-milling (B)					
Dried in air	652	282	1397	704	11.2
Calcination at 673 K	699	306	1555	823	8.5
Calcination at 773 K	871	403	1760	860	7.8
Calcination at 873 K	822	385	1837	850	6.2

Photocatalytic reaction: catalyst 0.5 g; 450 W Hg lamp; H_2O 330 cm^3.
BET mesurements: All samples were evacuated at 473 K for 2 h and mesurements were undertaken by N_2 adsorption at 77 K.

tocatalytic activity increased with increasing the calcination temperature. Both reached a maximum at 773 K, exceeding that of the original $K_4Nb_6O_{17}$. In the case of Ni (1.0 wt%) loading, those milled catalysts showed much higher activity even without calcination, and the activity was also increased by calcination before Ni loading. The dependence of the activity upon calcination temperature is interpreted as follows. Disordering and defect formation in $K_4Nb_6O_{17}$ particles occurred somewhat during ball-milling treatments. Then calcination in air is considered to recover the ordering to some extent. Therefore, the photocatalytic activity was increased by calcination regardless of the decrease in surface area.

Figure 5 shows the dependence of the rate of H_2 evolution from water upon the amount of loaded Ni over the milled (A) and milled (B), both calcined at 773 K, and the original $K_4Nb_6O_{17}$. As mentioned above, the highest activity of the original $K_4Nb_6O_{17}$ was obtained with the Ni loading of 0.1 wt% when a reaction vessel made of Pyrex® was used. In the study of this section, a quartz reaction cell was used and the optimum amount of loading Ni was shifted to 0.5 wt%. One difference of the Pyrex® from the quartz cells was transmittance of UV-light irradiated on the catalysts during the reaction, and the latter transmits the light of much shorter wavelength (> 200 nm) than the former (> 300 nm). The highest activities of both milled catalysts were obtained at 1.0 wt% of Ni loading, and then the rates of H_2 and O_2 evolution were 1608 and 789 $\mu mol\,h^{-1}$ for milled (A) and 1760 and 860 $\mu mol\,h^{-1}$ for milled (B), respectively. By comparison with that of the original one (890 and 445 $\mu mol\,h^{-1}$ with 0.5 wt% loading), the activity increased by 1.8—2.0 times. The larger amount of the optimun Ni loading for the catalyst of smaller particle size is due to its higher surface area.

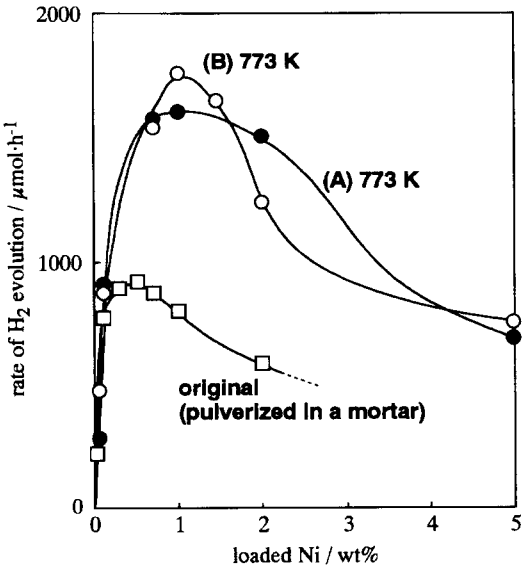

Fig. 5. Dependence of the rates of H_2 evolution from water upon the amount of loaded nickel over the original $K_4Nb_6O_{17}$, the milled (A) calcined at 773 K for 6 h and the milled (B) calcined at 773 K for 6 h. Catalyst 0.5 g; 450 W Hg lamp; H_2O 330 cm^3.

1.2(b). Smaller Size of $K_2La_2Ti_3O_{10}$ Prepared by Polymerized Complex.[11] $K_2La_2Ti_3O_{10}$ was prepared by the polymerized complex (PC) method, and its photocatalytic activity of water splitting was compared with the activity of that prepared by the conventional solid state reaction method. The PC method is known as the Pechini method.[12] It is based on polymerization between ethylene glycol (EG) and citric acid (CA) in the presence of soluble metal–CA complexes; the complexes are immobilized in a rigid polyester network almost in molecular level as in the original solution. Immobilization of the metal complexes can inhibit hydrocomplexation of the individual metal cations that might occur in the alkoxide-based sol–gel techniques. The starting materials for PC synthesis of $K_2La_2Ti_3O_{10}$ are $Ti[OCH(CH_3)_2]_4$, $La(NO_3)_3{\cdot}6H_2O$, and K_2CO_3. The addition of an over-stoichiometric amount of potassium to the "K/La/Ti CA/EG" solution was necessary to compensate for the volatization of potassium during calcination. Figure 6 shows XRD patterns of the K/La/Ti = 4/2/3 composition precursor (containing 100 % excess amount of potassium) and of that calcined in air at temperatures between 873 and 1223 K. $La_{2/3}TiO_3$ phase primarily evolved at 873 K (Fig. 6(b)) but $K_2La_2Ti_3O_{10}$ formed as a main phase at 1073 K for 2 h, accompanied with the decrease of $La_{2/3}TiO_3$ phase (Fig. 6(c)). As shown in diffraction patterns in Fig. 6 ((d), (e), (f), and (g)), pure $K_2La_2Ti_3O_{10}$ could be obtained by calcination at 1073 K for 12 h or at higher temperatures between 1123 and 1223 K for 2 h. If one compares the product prepared at the same temperature by the PC method and the conventional solid state reaction method, one finds that the former product crystallized better than the latter. This indicates that the PC method has a considerably higher crystallization rate than

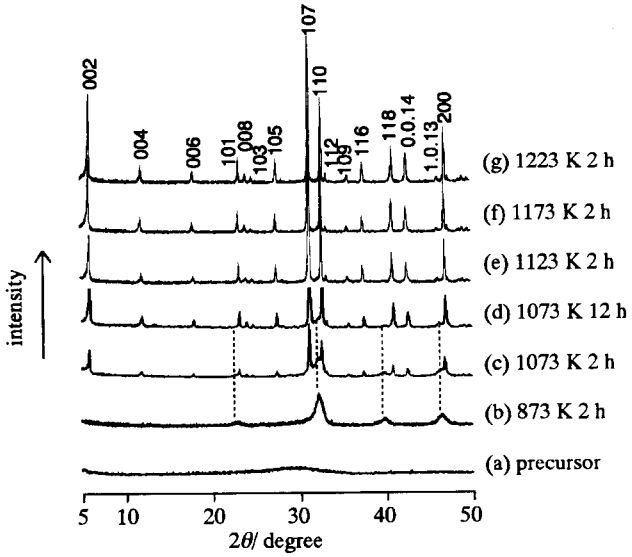

Fig. 6. XRD patterns of the precursor containing 100% excess of potassium (K/La/Ti = 4/2/3) (a) and that heated in air at 873 K for 2 h (b), at 1073 K for 2 h (c), at 1073 K for 12 h (d), at 1123 K for 2 h (e), at 1173 K for 2 h (f), and at 1223 K for 2 h (g). The diffractions on dotted lines are attributed to $La_{2/3}TiO_3$.

the conventional solid state reaction method.

Table 3 lists the photocatalytic activities of water decomposition upon NiO/Ni(3 wt%) loaded $K_2La_2Ti_3O_{10}$ prepared by the PC method at temperatures between 1073 and 1223 K, with their BET surface areas measured by N_2 adsorption at 77 K. The highest activity was achieved by the sample calcined at 1173 K for 2 h. The photocatalytic activity decreased with increasing the preparation temperature from 1173 to 1223 K. Such decrease of the activity is probably due to the decrease of the surface area. In this context, the samples prepared at lower calcination temperatures (1073 K for 12 h and at 1123 K for 2 h) were expected to exhibit higher activities because their surface area was much larger than the area of that prepared at 1173 K for 2 h. However, the samples prepared at 1073 and 1123 K show lower photocatalytic activity. Figure 7 shows the SEM photographs of the catalysts prepared by the PC method at temperatures between 1073 and 1223 K. The morphology of the sample calcined at 1073 K for 12 h (Fig. 7(a)) is granular, and individual particles could not be distinguished, while individual particles of the sample calcined at 1123 K for 2 h (Fig. 7(b)) are clearly distinguishable thabks to the uneven surface. In the cases of the samples calcined at 1173 and 1223 K for 2 h (Figs. 7(c) and 7(d)), a smooth surface and a square shape are observed for each particle. From the SEM measurements, the surfaces of the samples calcined at 1073 and 1123 K seem not to be well crystallized. Furthermore, the products prepared at 1073 K for 12 h and at 1123 K for 2 h contain $La_{2/3}TiO_3$ phase that is inactive for photocatalytic water splitting. These samples show much lower photocatalytic activities than expected from those with relatively large surface areas. For well-crystallized $K_2La_2Ti_3O_{10}$ samples, however, the photocatalytic activity depends strongly on the surface. The photocatalytic activities of the catalysts prepared by the solid state reaction method and each BET surface area are also summarized in Table 4. Comparing the catalyst prepared by heating the "K/La/Ti = 2.6/2/3" mixture at 1173 K for 72 h with that prepared at 1323 K for 48 h, one sees that the former has higher activity than the latter, as expected from the larger surface area of the former one.

Table 3. Dependence of Photocatalytic Activity and BET Surface Area of NiO/Ni–$K_2La_2Ti_3O_{10}$ (PC) upon Calcination Temperature

Calcination temperature/K[a]	Rate of gas evolution μmol h^{-1}		BET surface area (m^2 g^{-1})
	H_2	O_2	
1073[b]	528	264	54
1123	1316	537	22
1173	2186	1131	5
1223	1042	427	3

a) Calcination for 2 h. b) For 12 h.

Figure 8 shows the time courses of H_2 and O_2 evolution of the most active catalysts prepared by the PC method (calcined at 1173 K for 2 h) and of that prepared by the conventional

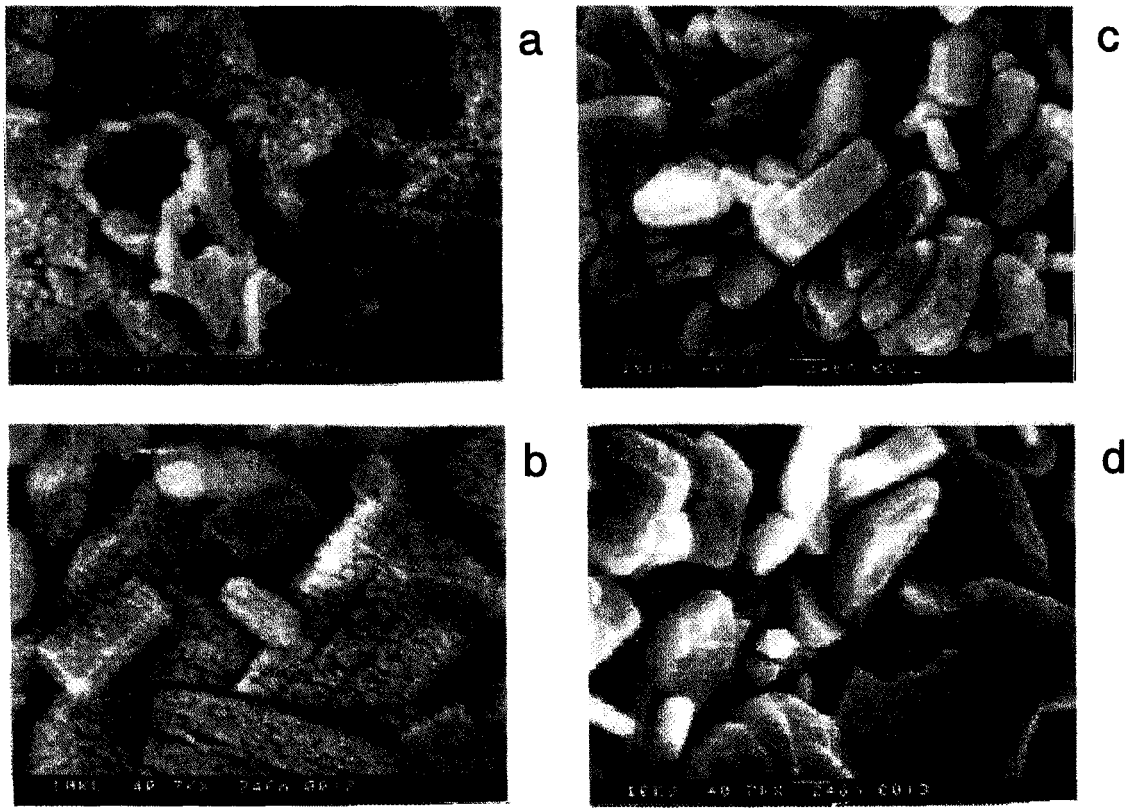

Fig. 7. SEM photographs of $K_2La_2Ti_3O_{10}$ prepared by the PC method at 1073 K for 12 h (a), at 1123 K for 2 h (b), at 1173 K for 2 h (c), and at 1223 K for 2 h (d).

Table 4. Photocatalytic Activities of NiO/Ni–$K_2La_2Ti_3O_{10}$ Prepared by the Conventional Solid State Reaction

Preparation method	Rate of gas evolution $\mu mol\ h^{-1}$		BET surface area ($m^2\ g^{-1}$)
	H_2	O_2	
(30% excess of K[a]) at 1173 K for 72 h	1255	632	4
(30% excess of K[a]) at 1323 K for 48 h	583	270	1
(stoichiometric[b]) at 1323 K for 48 h	444	220	1

a) Prepared from the mixture containing 30% excess of K (K/La/Ti = 2.6/2/3). b) prepared from the stoichiometric mixture (K/La/Ti = 2/2/3).

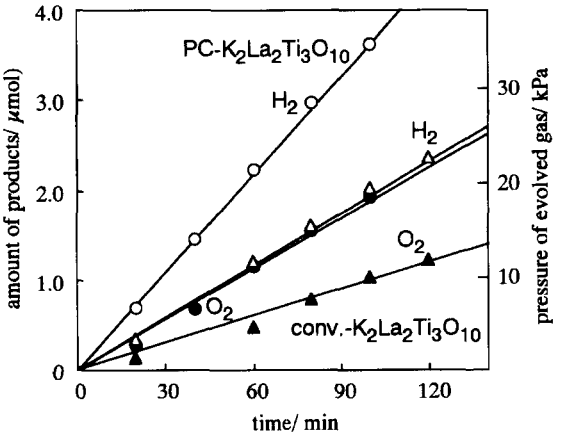

1 g catalyst
300 ml aqueous KOH (0.1 M)
high pressure Hg lamp (450 W) light source
inner irradiation type quartz reaction cell.

Fig. 8. Time course of gas evolution over the PC- $K_2La_2Ti_3O_{10}$/Ni catalyst and the conventional-$K_2La_2Ti_3O_{10}$/Ni catalyst: 1 g catalyst; 300 ml aqueous KOH (0.1 M); high pressure Hg lamp (450 W) light source; inner irradiation type quartz reaction cell.

solid state reaction method (calcined at 1173 K for 72 h). The PC–NiO/Ni–$K_2La_2Ti_3O_{10}$ shows double the photocatalytic activity of the conventional–NiO/Ni–$K_2La_2Ti_3O_{10}$. The difference of the activity in preparation methods may not be explained only by the surface areas, because the difference in surface area is much smaller (5 and 4 $m^2\ g^{-1}$, respectively) than that in activity. It is noted that the UV-vis DR (diffuse reflectance) spectrum of the conventional $K_2La_2Ti_3O_{10}$ has a shoulder peak in a wavelength region of about 350—450 nm. Although the assignment of the additional absorption is not clear, it may be attributed to some defect such as a non-stoichiometric part and it may act as a recombination center for photogenerated electron-hole pairs. These results indicate that a well-crystallized catalyst with higher surface area and/or smaller particle size shows higher activity for overall water splitting, as summarized in Table 4.

1.2(c). Reconsideration of the Reaction Models. Based on the reaction schemes previously proposed by the authors for the photocatalysts with layered structures (Figs. 2(a) and 2(c)), we conclude that the hydrated interlayer spaces work as reaction sites. Two examples described above (i.e. $K_4Nb_6O_{17}$ and $K_2La_2Ti_3O_{10}$), however, enforce us to improve the models to some extent. The results indicate that smaller particles give higher activity for overall water splitting reaction if the layered oxides are well-crystallized. In the original model of Ni/$K_4Nb_6O_{17}$ (Fig. 2(a)), photoexcited electrons and holes react at the different sides of the niobate sheet, and the particle size does not affect the efficiency for the overall water splitting in principle. The dependence of the activity on the particle size may indicate that the photons absorbed near the edge plane are utilized more efficiently than those apart from the edge plane.

One of the possible explanations of this result is as follows: When electrons and holes react at the interlayer spaces I and II, OH^- and H^+ species remain at the interlayer spaces I and II, respectively, which causes a reverse bias against the charge separation. To recover from this situation, produced OH^- and H^+ species have to migrate into a solution phase to recombine into water molecules. This process must be easier for the species generated near the edge plane than for those deep inside of the catalyst. This eventually causes the decrease of the efficiency of larger particles. This model also explains the dependence of the quantum efficiency on the wavelength, i.e. the photons with wavelength near the absorption edge are less effective than those with shorter wavelengths. The light with the wavelength near the absorption edge tends to penetrate deeper into the catalyst than those with shorter wavelength because the absorbance of the light is larger for the shorter wavelength light. The higher quantum efficiency for the light with shorter wavelength is a consequence of the process mentioned above.

Another possible explanation is as follows: in the original model, the loaded ultrafine nickel metal particles are supposed to be dispersed homogeneously within the catalyst powder. If this is the case, the optimum amount of the loaded nickel should be the same regardless of the particle size. However, Fig. 6 clearly shows that the optimum amount of nickel loading depends on the particle size, i.e. for smaller particles, the optimum loading is larger. This indicates that loaded nickel metal particles are not dispersed homogeneously in the catalyst but preferentially locate near the edge plane. As a consequence, the region near the surface catalyzes the overall water splitting more efficiently than the inside of the catalyst where the nickel particles are insufficiently loaded. When the particle size of the catalyst becomes smaller, the relative amount of the more efficient region with enough nickel metal particles increases and this results in the increase of the optimum loading of nickel.

1.3. New Photocatalysts Based on Ta-Containing Materials. The photocatalysts for overall water splitting introduced above consist of Ti- or Nb-containing mixed oxides. Some Ta-containing oxides have recently been found by Kudo's group to be active for overall decomposition of water.[13—17] One of the Ta-based oxides, $K_3Ta_3Si_2O_{13}$, was first found to show the photocatalytic activity for overall

water decomposition. Following this, various other Ta-containing oxides were also found to be active, as summarized in Table 5. All of the catalysts in Table 5 decompose pure water into H_2 and O_2 even without any co-catalysts, and the activities are enhanced by NiO-loading. NiO-loaded $NaTaO_3$ showed the highest activity among them. The substitution of Ta site by Zr^{4+} ion in $KTaO_3$ resulted in the stoichiometric water decomposition.[18] One of the characteristic features of the group of Ta-containing photocatalyst is that the high activity is attained in pure water without R773–O473 pretreatment, which is introduced below.

Some new information on the mechanism of photocatalytic water decomposition was given by comparison of $Sr_2Ta_2O_7$ and $Sr_2Nb_2O_7$ which possess the same layered perovskite structure. The band gap energy appears higher for $Sr_2Ta_2O_7$ than for $Sr_2Nb_2O_7$ (Table 5).[13–18] The difference is mainly due to the orbitals forming conduction bands: the conduction band of $Sr_2Ta_2O_7$ consists of Ta_{5d}, while that of $Sr_2Nb_2O_7$ is Nb_{4d}. The valence band potential of $Sr_2Ta_2O_7$ should be similar to that of $Sr_2Nb_2O_7$ because the valence bands consist of O_{2p} orbitals and because the oxygen anions coordinate to Ta^{5+} or Nb^{5+} with the same ionic radius. The band structures of $Sr_2Ta_2O_7$ and $Sr_2Nb_2O_7$ can be roughly described as shown in Fig. 9, together with that of NiO.[19] O_2 evolution on $Sr_2Ta_2O_7$ and $Sr_2Nb_2O_7$ is regarded as equally easy, because of the sufficient depth of the potentials of their valence bands to oxidize water into O_2. Therefore, the higher photocatalytic activity of $Sr_2Ta_2O_7$ than that of $Sr_2Nb_2O_7$ is attributed to the difference in the conduction band level. The ability of

Table 5. Photocatalytic Activity for Overall Water Decomposition over Various Tantalates

Photocatalyst	NiO	Band gap	Activity / μmol h^{-1}		Ref.
	wt%	eV	H_2	O_2	
$NaTaO_3$	None	4.0	161	88	13
$NaTaO_3$	0.05	4.0	2180	1100	13
$KTaO_3$ [a)]	1.50	—	122	57	18
$CaTa_2O_6$	None	4.0	21	8.3	14
$CaTa_2O_6$	0.10	4.0	72	32	14
$SrTa_2O_6$	None	4.4	140	60	14
$SrTa_2O_6$	0.10	4.4	629	303	14
$BaTa_2O_6$	None	4.1	33	15	15
$BaTa_2O_6$	0.30	4.1	960	490	15
$ZnTa_2O_6$	0.10	4.4	15	6	15
$NiTa_2O_6$	None	3.7	11	4	15
$Sr_2Ta_2O_7$	None	4.6	52	18	16
$Sr_2Ta_2O_7$	0.15	4.6	1000	480	16
$Sr_2Nb_2O_7$	0.5	3.9	10	3.2	16
$Sr_2Nb_2O_7$	0.5[b)]	3.9	110	36	16
$K_3Ta_3Si_2O_{13}$	None	4.1	43	19	17
$K_3Ta_3Si_2O_{13}$	1.30	4.1	368	188	17

a) After R673–O773 pretreatment, and 8 mol% of Ta was substituted by Zr^{4+}. b) After R773–O473 pretreatment.

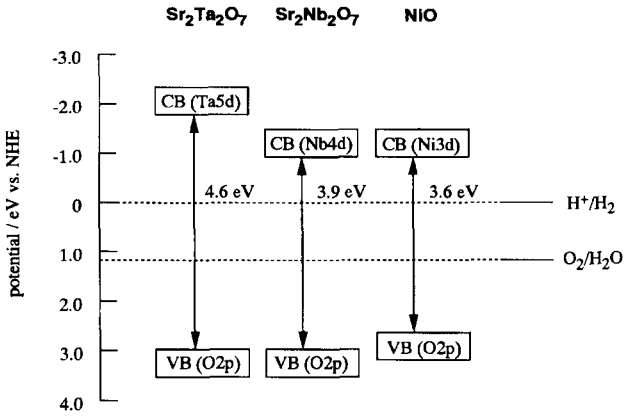

Fig. 9. Band structures of $Sr_2M_2O_7$ (M = Nb and Ta) photocatalysts and NiO co-catalyst. The conduction band levels of $Sr_2Ta_2O_7$ and $Sr_2Nb_2O_7$ are approximated to the flat band potentials because they are n-type semiconductors.

$Sr_2Ta_2O_7$ for the decomposition of pure water without co-catalysts is also interpreted by its high conduction band level which is advantageous for H_2 evolution in addition to the surface catalytic ability for H_2 evolution.

In general, R773–O473 pretreatment is indispensable for obtaining high activities for NiO-loaded photocatalysts as mentioned in Section 1.1(a). The surface NiO works as a H_2 evolution site, and the electrons photogenerated in photocatalysts have to cross the interface between photocatalysts and the loaded NiO co-catalyst to reach the NiO surface. In this case, the existence of Ni metal lowers the barrier for the electron crossing from oxide photocatalyst to NiO. Thus, R773–O473 pretreatment assists the electron transfer from photocatalysts to NiO co-catalysts.[2,3] This pretreatment was indispensable for $NiO/Sr_2Nb_2O_7$, whereas it was not for $NiO/Sr_2Ta_2O_7$. In the case of the nontreated $NiO/Sr_2Ta_2O_7$ photocatalyst, electrons can transfer even at the interface between oxides because of the high conduction band level which results in high activity even without pretreatment. In other words, the photogenerated electrons in a conduction band of $Sr_2Ta_2O_7$ can transfer to a conduction band of NiO, as shown in Fig. 9. In contrast, the negligible potential difference in the conduction band between $Sr_2Nb_2O_7$ and NiO requires the R773–O473 pretreatment similarly to the case of $NiO/SrTiO_3$.[2]

1.4. New Visible-Light-Driven Photocatalysts. Some wide band gap photocatalysts have been found to be highly active for splitting water into H_2 and O_2 in stoichiometric amounts under UV irradiation, as mentioned above. However, photocatalysts which can efficiently split water into H_2 and O_2 by visible light irradiation have never been found so far. Even in the presence of sacrificial reagents, the only well-known photocatalyst which is active for H_2 evolution under visible light irradiation is Pt/CdS (BG = 2.4 eV).[1,20] On the other hand, WO_3 (BG = 2.8 eV)[1,20] is a well-known photocatalyst which is active for O_2 evolution under visible light irradiation in the presence of electron acceptors such as Ag^+ and Fe^{3+} (Fig. 11) Kudo and co-workers have recently reported some new visible-light-driven photocat-

alysts. CuS–ZnS solid solution photocatalysts (BG = 2.5 eV) prepared by a coprecipitation method are active for H_2 evolution under visible light irradiation in aqueous K_2SO_3 solutions,[3] as shown in Fig. 10. On the other hand, $BiVO_4$ prepared by the reaction of layered potassium vanadate powder (KV_3O_8 and $K_3V_5O_{14}$) with $Bi(NO_3)_3$ for 3 d in aqueous media at room temperature is more active than WO_3, as shown in Fig. 11.[22,23] Highly crystalline monoclinic and tetragonal $BiVO_4$ were selectively synthesized by changing the ratio of vanadium to bismuth in the starting materials on the novel aqueous process. The tetragonal $BiVO_4$ with a 2.9 eV band gap mainly possesses an ultraviolet absorption band, while monoclinic $BiVO_4$ with a 2.4 eV has a characteristic visible light absorption band in addition to the UV band, as shown in Fig. 12. The monoclinic $BiVO_4$ shows high photocatalytic activity for the O_2 evolution from aqueous silver nitrate solutions under visible light irradiation (wavelength > 420 nm). The visible light response was attributed to the band transition from hybrid Bi_{6s}–O_{2p} orbitals to V_{3d}.

Layered perovskite type niobates are also good photocatalysts. From aqueous methanol solution, they evolve hydrogen efficiently as shown in Table 6. In aqueous silver nitrate solution, O_2 evolution was also observed for each catalyst, as shown in Table 6. Thus these layered perovskites have a potential for overall water splitting as in the case of $A_4Nb_6O_{17}$ if proper modifications are made. It is further noted that this type of layered perovskites has many relatives.[24] Especially, when various cations are substituted for M atoms in the niobate sheet of $A(M_{n-1}Nb_nO_{3n+1})$, some of them show an absorption band extended into the visible light region. Among them, $RbPb_2Nb_3O_{10}$ was found to have some photocatalytic activity under visible light irradiation. This material is not hydrated in the original form, while it is hydrated by the substitution of protons for interlayer Rb^+ ions. The structure of this triple oxide is the same as that drawn for $n = 3$ in Fig. 13 (A = Rb, M = Pb). The diffuse reflectance spectrum of ultraviolet-visible light region is shown in Fig. 14 as well as those of $K_4Nb_6O_{17}$ and $KCa_2Nb_3O_{10}$.[24] The rates of photocatalytic evolution of H_2 on several $RbPb_2Nb_3O_{10}$-based catalysts from aqueous methanol solution (250 cm^3 water and 50 cm^3 methanol) were measured under the irradi-

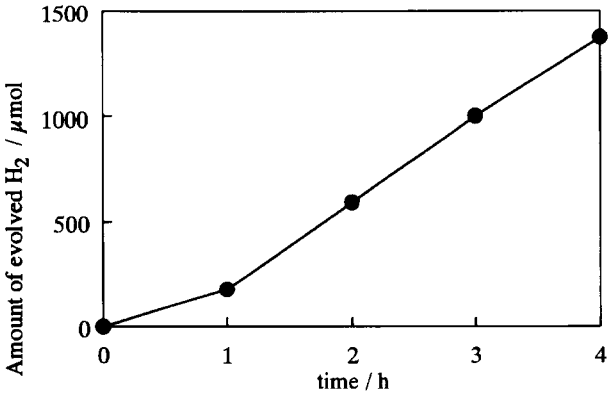

Fig. 10. Photocatalytic H_2 evolution from an aqueous Na_2SO_3 solution (0.5 M, 300 cm^3) under visible light irradiation (wavelength > 420 nm) over $Zn_{0.957}Cu_{0.043}S$. Light source: 300 W Xe lamp.

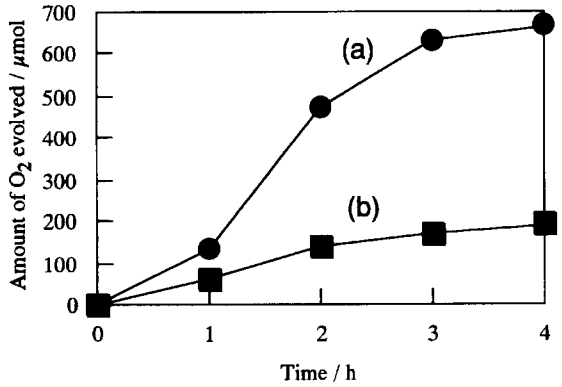

Fig. 11. Photocatalytic O_2 evolution from aqueous $AgNO_3$ solutions (0.5 M, 300 cm^3) under visible light irradiation (wavelength > 420 nm) on (a) monoclinic $BiVO_4$ synthesized from $K_3V_5O_{14}$ and (b) WO_3. Light source: 300 W Xe lamp.

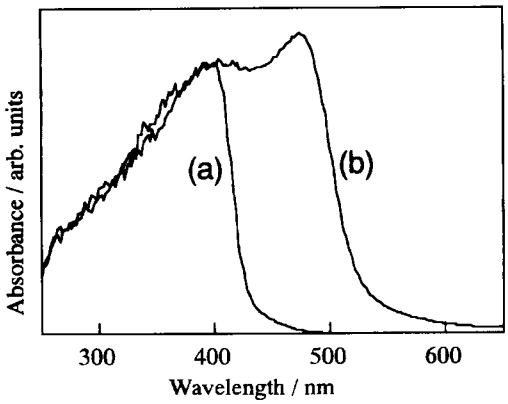

Fig. 12. Diffuse reflectance spectra of (a) tetragonal and (b) monoclinic $BiVO_4$ synthesized by the aqueous process from KV_3O_8 and $Bi(NO_3)_3$.

Table 6. Photocatalytic Activities of Layered Perovskite Compounds; $A[M_{n-1}Nb_nO_{3n-1}]$

		Rate of gas evolution / μmol h^{-1}				
		H_2 [a]				O_2 [b]
		Original		H^+-exchanged [c]		
Catalyst	n	Alone	Pt-loaded [d]	Alone	Pt-loaded [d]	
$KLaNb_2O_7$	2	28	54	760	3800	46
$RbLaNb_2O_7$	2	60	90	740	2600	2
$CsLaNb_2O_7$	2	12	28	300	2200	3
$KCa_2Nb_3O_{10}$	3	14	100	5900	19000	8
$RbCa_2Nb_3O_{10}$	3	3	26	3100	17000	16
$CsCa_2Nb_3O_{10}$	3	2	10	970	8300	10
$KSr_2Nb_3O_{10}$	3	10	110	8900	43000	30
$KCa_2NaNb_4O_{13}$	4	5	280	790	18000	39

Catalyst 1.0 g, high pressure Hg lamp (450 W), a) MeOH 50 ml + H_2O 300 ml, b) 0.01 M $AgNO_3$ aq 350 ml, c) H^+-exchange degree > 95%, d) Pt was loaded from H_2PtCl_6 aq by photodeposition method. The amounts of loading were 0.1 wt%.

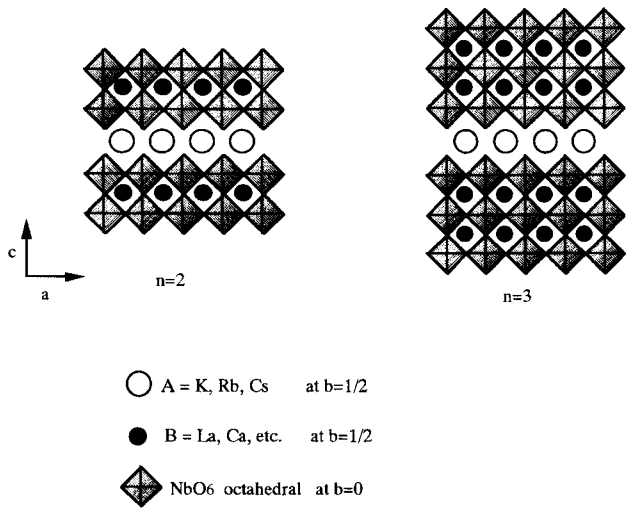

Fig. 13. Schematic structure of layered perovskites.

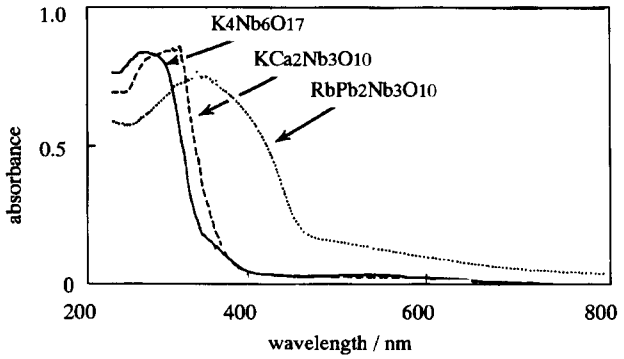

Fig. 14. Ultraviolet-vis. diffuse reflectance spectra of various niobate compounds.

ation with a xenon-lamp through a cut off filter (> 420 nm). Time courses of H_2 evolution from aqueous methanol solution under visible light (> 420 nm) irradiation over a series of $RbPb_2Nb_3O_{10}$-based catalysts are shown in Fig. 15. The activity is enhanced by two to three orders of magnitude due to exchanging Rb^+ in the interlayers to H^+, while the original catalyst showed the low photocatalytic activity. Further enhancement of the activity was achieved by Pt loading.

For Pt loading, two types of precursors, $[Pt(NH_3)_4]Cl_2$ and H_2PtCl_6, were used. These were photoreduced to Pt metal particles under the reaction conditions. The induction period observed for H_2 evolution is due to the reduction to Pt. Between the two precursors, the former gave the catalyst with much higher activity. As $RbPb_2Nb_3O_{10}$ is a cation exchanger, it is expected that $[Pt(NH_3)_4]^{2+}$ ions will intercalate into the interlayers, while negatively charged $PtCl_6^{2-}$ ions are unable to migrate into interlayers. As a result the photoreduced Pt may exist at the interlayer space in the former case and at the external surface in the latter case. The photoexcited electrons in the bulk of catalyst should migrate to the external Pt particles in order to efficiently reduce protons and to evolve H_2. During the migration of electrons, some of them should be consumed by the recombination with the simultaneously generated holes. This is the origin of the low

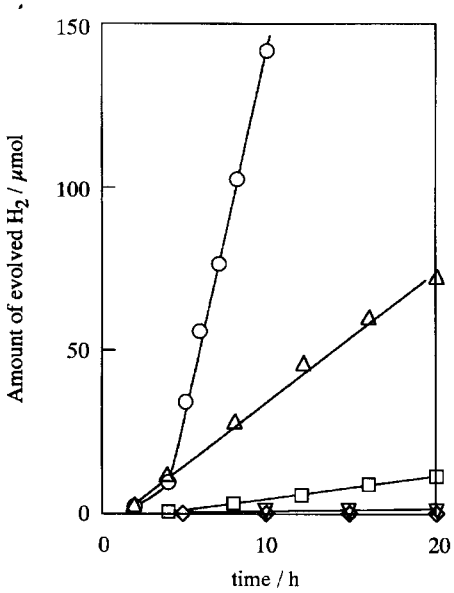

Fig. 15. Time courses of visible light induced H_2 evolution from an aqueous methanol solution (17 vol%, 250 cm^3 water and 50 cm^3 methanol) over several modified $RbPb_2Nb_3O_{10}$ catalysts. ◇: $RbPb_2Nb_3O_{10}$, ▽: Pt (0.1 wt%)/$RbPb_2Nb_3O_{10}$ (H_2PtCl_6), □: $HPb_2Nb_3O_{10}$, △: Pt (0.1 wt%)/$HPb_2Nb_3O_{10}$ (H_2PtCl_6), ○: Pt (0.1 wt%)/$HPb_2Nb_3O_{10}$ ($[Pt(NH_3)_4]Cl_2$). Light sourse: 300 W Xe lamp (> 420 nm).

activity of the Pt-loaded catalyst from H_2PtCl_6. On the other hand, recombination of photogenerated electrons and holes decreased on the highly-dispersed Pt-loaded catalyst prepared by $[Pt(NH_3)_4]Cl_2$ precursor. The structures of both Pt-loaded catalysts were confirmed by XPS and TEM measurements. The sample prepared from H_2PtCl_6 clearly exhibited Pt_{4d} peaks by XPS while that prepared from $[Pt(NH_3)_4]^{2+}$ did not. This indicates that there exists a larger amount of Pt on the surface of the former catalyst than the amount of the latter material. Moreover, Pt particles of 5—10 nm in diameter were observed only in the TEM photograph of the former sample. The structures inferred from the above results are schematically depicted in Fig. 16. The sample obtained from $[Pt(NH_3)_4]Cl_2$ contains ultrafine Pt particles in interlayers. The higher efficiency of H_2 evolution is, therefore, considered to be due to the shorter transportation distance of excited electrons to ultrafine Pt particles than that to Pt on the external surface.

It is interesting to study the rate of ion exchange reaction between H^+ and $Pt(NH_3)_4^{2+}$ cations. In Fig. 17, rates of H_2 evolution were plotted against the treatment time of $HPb_2Nb_3O_{10}$ in aqueous methanol solution containing Pt precursor complexes. When $[Pt(NH_3)_4]Cl_2$ was used as a Pt precursor, the rate of H_2 evolution increased with the treatment time and reached a maximum after a week at 353 K. For H_2PtCl_6, no dependence of the activity on the treatment time was observed. This implies that the rate of ion-exchange between H^+ and $[Pt(NH_3)_4]^{2+}$ is relatively slow. It is another interesting question whether this catalyst evolves O_2 under visible light irradiation. A constant rate of O_2 evolu-

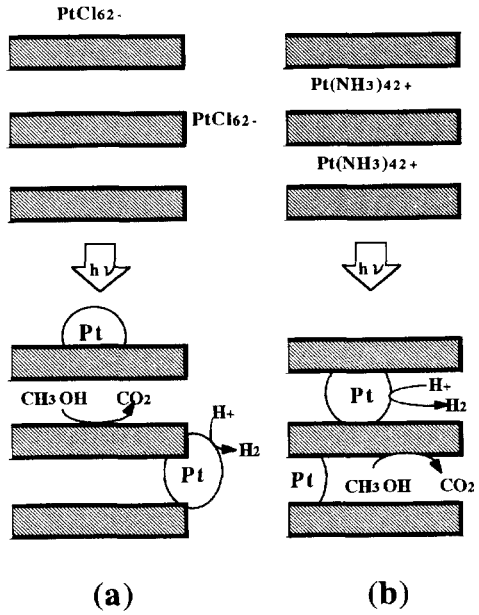

Fig. 16. Schematic mechanism of H_2 evolution over a $Pt/HPb_2Nb_3O_{10}$. (a) Pt exists only on the external surfaces, (b) Pt exists in the interlayers.

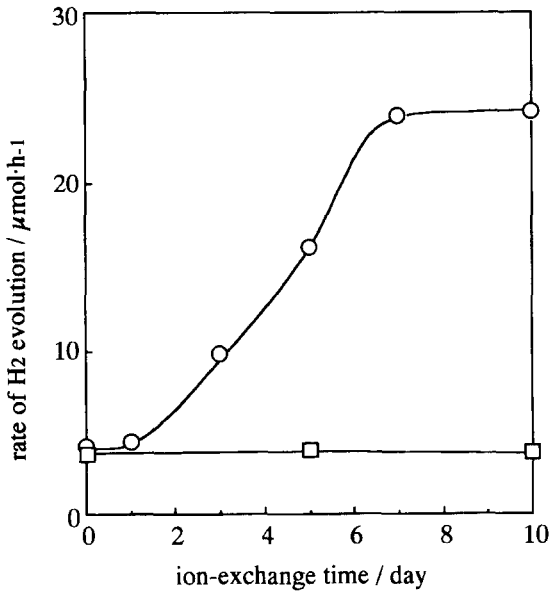

Fig. 17. Rate of H_2 evolution as a function of the treatment time of $HPb_2Nb_3O_{10}$ in an aqueous solution containing a Pt precursor. ○: $[Pt(NH_3)_4]Cl_2$, □: H_2PtCl_6. Pt (0.1 wt%) was fixed on the catalyst. 500 W Xe lamp (> 420 nm), catalyst 1 g, CH_3OH (50 ml)+H_2O (250 ml).

tion (1.1 μmol h^{-1}) from aqueous silver nitrate solution was observed for original $RbPb_2Nb_3O_{10}$ while no O_2 evolution was observed for $HPb_2Nb_3O_{10}$, as shown in Table 7. The deficiency of O_2 evolution in the case of $HPb_2Nb_3O_{10}$ may be due to the acidic property of the interlayer space, which suppresses the O_2 formation.

1.5. Detailed Reaction Mechanism for the Initial Charge Separation in Photocatalytic Overall Water Splitting. Predictions about the availability of the overall water decomposition have been very difficult. Under such a circumstance, the importance of the relation of the photocatalytic activity for overall water decomposition with the lattice distortion is recently proposed. This proposal is not yet applied generally, but it would become a profitable guideline for exploring catalysts.

Table 7. Photocatalytic Activities of Several Modified $RbPb_2Nb_3O_{10}$ Catalysts

Catalyst	Rate of gas evolution / μmol h^{-1}		
	H_2[a]		O_2[b]
	Alone	Pt-loaded[c]	
Original	0	0.1	1.1
H^+-exchanged	0.59	3.7	0

Catalyst 1.0 g; 500 W Xe lamp (> 420 nm); a) H_2O (250 ml) + methanol (50 ml); b) 0.01 M $AgNO_3$ aq (250 ml) (1 M = 1 mol dm^{-3}); c) Pt was loaded from H_2PtCl_6 aq by photodeposition method. The amounts of loading were 0.1 wt%.

An efficient overall water splitting was found by Inoue et al. on RuO_2-loaded $BaTi_4O_9$ catalyst.[25] The main feature in the structure of $BaTi_4O_9$ is the pentagonal-prism tunnel structure (Fig. 18(a)). Results suggested that the distorted TiO_6 octahedra in pentagonal-prism tunnel structure is essential for an efficient H_2O decomposition. The tunnel structure serves the uniform distribution of RuO_2 particles. The pentagonal-prism tunnel space provides the form of a "nest", i.e., a concave site with a ridge in which a small RuO_2 particle firmly fits, as depicted in Fig. 19. The strong interaction between

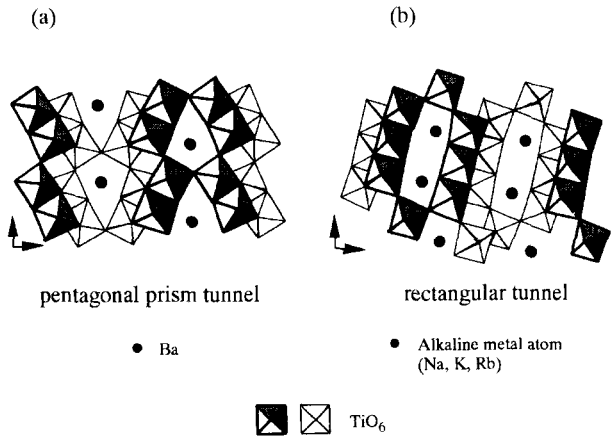

Fig. 18. Schematic structures of $BaTi_4O_9$ (a) and $M_2Ti_6O_{13}$ (b).

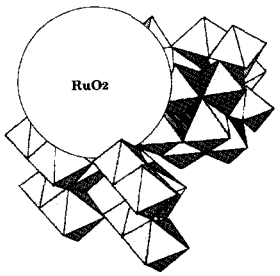

Fig. 19. The "nest" model for the local structure of $RuO_2/BaTi_4O_9$.

the small RuO_2 particle and the surrounding TiO_6 octahedra facilitates the transfer of photoexcited electrons and holes to the adsorbed species. This strong interaction was related to the distortion of the TiO_6 octahedra in the $BaTi_4O_9$ as shown below.

Inoue et al. studied the dependence of the photocatalytic activity for water decomposition on the calcination temperature of $BaTi_4O_9$ prepared by a sol–gel method. They concluded that calcination above 1173 K is necessary to activate $BaTi_4O_9$ catalyst.[26] This process was attributed to the formation of the active pentagonal-prism structure by XRD, TG-DTA (thermogravimetry-differential thermal analysis) and Raman spectroscopy. The most important result is the concurrent generation of EPR (electron paramagnetic resonance) signals (g = 2.018 and 2.004) due to O^- radicals when a series of $BaTi_4O_9$ catalysts calcined at different temperatures were irradiated by UV at 77 K under the atmosphere of O_2.[26] The intensity of EPR signals and the photocatalytic activity were in good accordance as shown in Fig. 20. The reliable correspondence of the photocatalytic activity for water decomposition and the emergence of EPR signals was further supported by their behavior against H_2 reduction and O_2 oxidation.[9] Reduction of $BaTi_4O_9$ decreased and reoxidation recovered the photocatalytic activity, where simultaneous increase and decrease of the EPR signals were quantitatively related.[9] Figure 21 shows the effect of reoxidation of the prereduced $BaTi_4O_9$ samples on their EPR signal intensity and the photocatalytic activity for overall water decomposition. Although reduction of $BaTi_4O_9$ reduces both EPR signal intensity and the photocatalytic activity, reoxidation at 1173 K of the samples reduced below 1123 K recovered them (Fig. 21(B)), while reoxidation at 773 K had little effect. Figure 21(A) also well demonstrates the gradual and simultaneous reduction of EPR signal intensity and the photocatalytic activity by increasing in reduction temperature. Some further quantitative evidence was given by the plot of the catalytic activity for H_2 and O_2 evolution as a function of EPR signal intensity (Fig. 22), where the linear dependence was obtained.[9] In this way, the active sites for photocatalytic water decomposition are proposed to be the same as those for radical formation. More importantly, $BaTi_4O_9$ is not the only case. For Wadsley–Andersson type oxides with a general formula, $M_2Ti_nO_{2n+1}$ (M denotes the alkali metal atoms), follow the above-mentioned relation of the photocatalytic activity with the intensity of the EPR signals.[27–31] $Na_2Ti_3O_7$ (n = 3) and $Na_2Ti_6O_{13}$ (n = 6) have a zig-zag and a rectangular tunnel structure, respectively as shown in Fig. 18(b). Both of them photodecompose water into the stoichiometric H_2 and O_2 when RuO_2 is highly dispersed as a co-catalyst,[27–31] and they also show EPR signals due to O^- radicals by UV irradiation at 77 K under O_2 atmosphere. The correlation of EPR and photocatalytic behaviors of $M_2Ti_6O_{13}$ (M = Na, K, Rb, and Cs) against reduction and reoxidation is also confirmed.[32,33] In addition, RuO_2 loaded barium titanates with a formula of

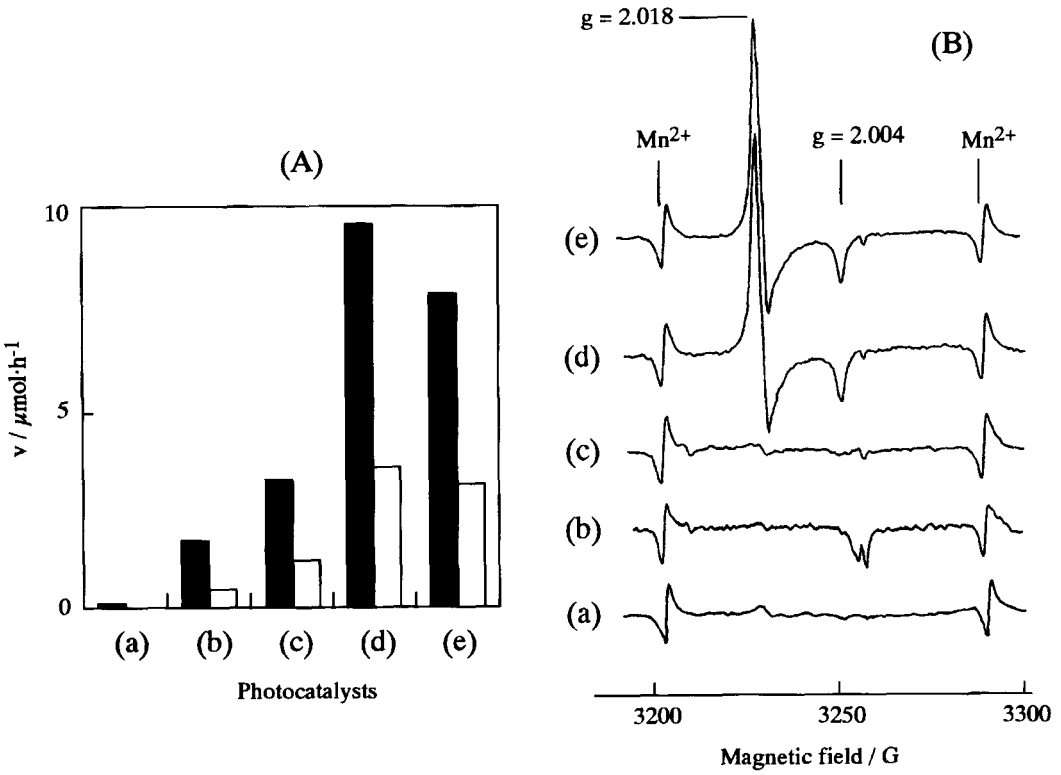

Fig. 20. Photocatalytic decomposition of water (B) and EPR spectra (A) of $BaTi_4O_9$ calcined at (a) 873 K, (b) 973 K, (c) 1073 K, (d) 1173 K, and (e) 1273 K. All the EPR spectra were measured with UV irradiation at 77 K in the presence of 30 Torr of O_2 (1 Torr = 133.322 Pa). 1 mass % of Ru was loaded as RuO_2 for measuring the photocatalysis. Filled and open bars show the rate of H_2 and O_2 evolution.

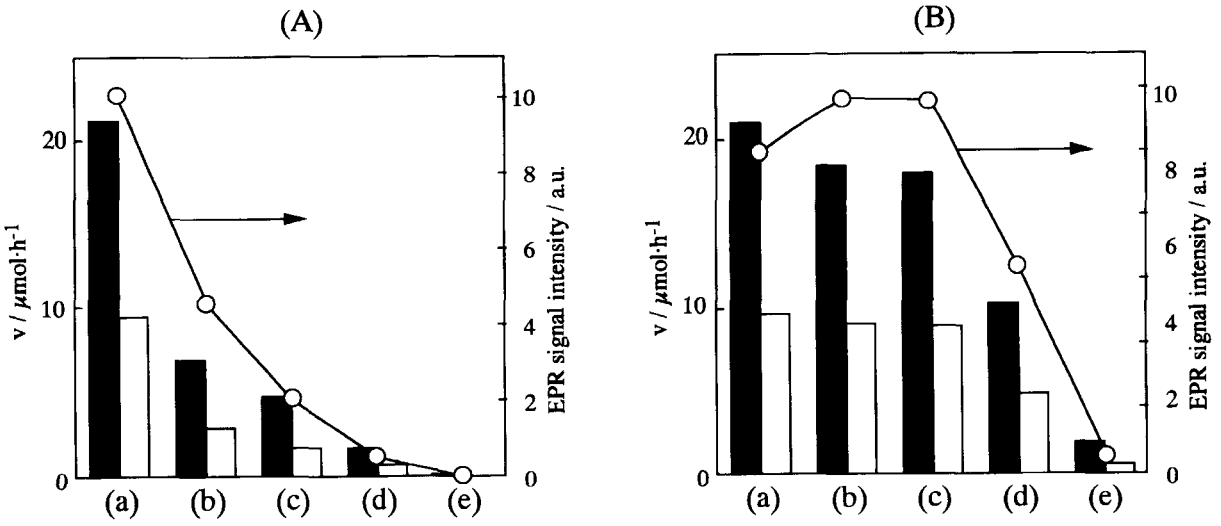

Fig. 21. Photocatalytic activity of 1.0 wt% RuO_2-loaded $BaTi_4O_9$ and EPR signal ($g = 2.018$) intensity. (a) denotes the original $BaTi_4O_9$ and other samples were reoxidized at 773 K after reduction at 1073 K (b), 1123 K (c), 1148 K (d), and 1173 K (e) in (A). The same prereduced samples were reoxidized at 1173 K in (B). Filled and open bars show the rate of H_2 and O_2 evolution.

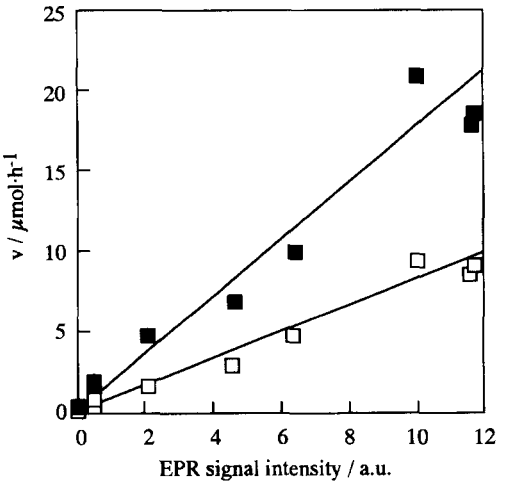

Fig. 22. Plots of photocatalytic activity as a function of the EPR signal intensity. ■: activity for H_2 production, and □: activity for O_2 production.

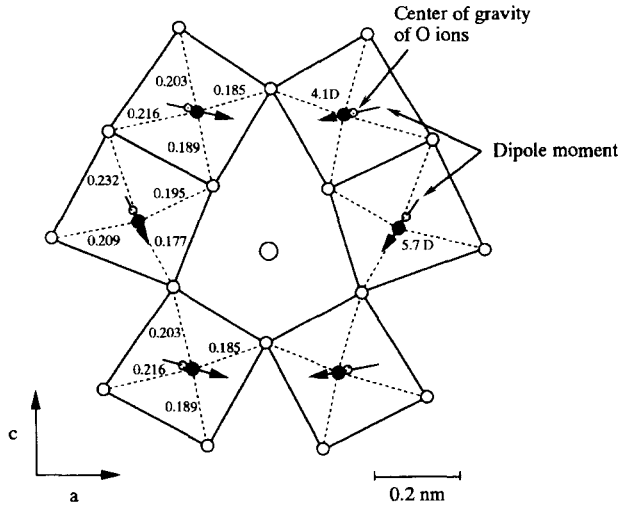

Fig. 23. A pentagonal-prism tunnel structure of $BaTi_4O_9$. Filled circle: Ti^{4+}; small circle: O^{2-}; large circle: Ba^{2+}; shaded circle: center of gravity. The arrows indicate dipole moments. The numbers express the Ti–O bond length in nm.

$Ba_{2(n-1)}Ti_{4n+1}O_{10n}$, ($n = 2$—4, $Ba_6Ti_{17}O_{40}$, $Ba_4Ti_{13}O_{30}$, and $Ba_2Ti_9O_{20}$) other than $BaTi_4O_9$ neither photodecompose water nor show EPR signals of O^- radicals due to the lack of any distorted lattice structure.[34]

The lattice distortion was found to be the origin of the photocatalytic activity and the generation of O^- radicals.[34,35] The O^- radicals arise from the lattice oxygen atoms in the distorted octahedra where high internal polarization fields due to dipole moment exist (Fig. 23). The dipole moments are, therefore, considered to work efficiently for the separation of photogenerated charges.

2. Mechanocatalytic Overall Water Splitting

Mechano-catalytic overall water splitting is a novel way to generate hydrogen from pure water by converting mechanical energy to chemical energy with the aid of some metal oxides. The phenomenological aspects of the mechano-catalytic overall water splitting will be reviewed, and the basic features of the catalytic process will be clearly established. The estimation of the energy conversion from mechanical to chemical is also shown. Next, some experimental results carried out to reveal the mechanism of the mechano-catalytic reaction are described. The reaction mechanism, which is still very speculative, will be discussed.

2.1. Introduction. During some research for developing photocatalytic systems to accomplish overall water splitting under visible light irradiation, it was accidentally found that some Cu(I)-containing oxides evolved H_2 and O_2 simultaneously from distilled water.[36] The reaction was first considered to be driven by the energy supplied from visible light photons. However, some unusual aspects were found judging from the conventional reaction mechanism of semi-

conductor-based photocatalytic reactions. For example, H_2 and O_2 evolution continued for a long period even after the irradiation stopped. Such a phenomenon was first interpreted as an energy reservation. Photoexcited electrons and holes reacted with the components of the oxide, in other words, the excited states were localized to form chemical species such as Cu(0) and O^- species. Then the chemical species gradually reacted with water to form H_2 and O_2. If this mechanism was correct, some amounts of H_2 and O_2 could be obtained after stopping the irradiation. In such a case, the amounts of evolved H_2 and O_2 should be much smaller than that of the catalyst employed, because no significant difference of the catalysts before and after the reaction was observed by several spectroscopic methods. To our surprise, however, the total molar amount of evolved gases in dark far exceeded that of the catalyst in carefully controlled reactions. On the other hand, when magnetic stirring of the catalyst was stopped, no evolution of H_2 and O_2 occurred. Thus, we realized that the H_2 and O_2 evolution is not due to a photocatalytic reaction but to some other mechanism that had been missed.

From various kinds of experimental results that will be described below, we named this somewhat curious reaction as "mechano-catalytic" overall water splitting.[37—41] In this reaction, mechanical energy is converted into chemical energy to form H_2 from water. Some phenomenological aspects of "mechano-catalytic" overall water splitting will be reviewed. The reaction mechanism is still not fully understood, but several possibilities will be discussed based on some experimental results. Most experimental results shown in this review have been published in our previous papers.

2.2. Reaction System.[39] The mechano-catalytic reaction was carried out in a flat-bottomed reaction vessel made of Pyrex glass. Typically, 0.1 g of metal oxide powder was suspended by magnetic stirring (F-205, Tokyo Garasu Kikai) in 200 cm^3 of distilled water. The stirring rod was sealed by PTFE (polytetrafluoroethylene, Tefron®). A closed gas circulation and evacuation system made of Pyrex® glass was connected to the reaction vessel. Evolved gases were accumulated in it (350 ml) for a gas chromatography analysis without any contamination of air (Fig. 24). The gas phase was evacuated to remove N_2 and O_2 prior to reactions, and to let only water vapor remain. When performing a dark reaction, the reaction vessel was completely covered with aluminum foil, and when performing the reaction under photoirradiation, a xenon lamp of 500 W placed at the side of the reaction vessel was used.

2.3. Experimental Results. As will be shown below, mechano-catalytic overall reaction is driven only by mechanical energy, and no photo-irradiation effect is observed for any of the mechano-catalysts except Cu_2O. In the case of Cu_2O, the band-gap irradiation affects the rates of H_2 and O_2 evolution to some extent, which previously caused misunderstanding of the reaction mechanism. It is now obvious that no photon energy is converted into chemical energy on Cu_2O even under band-gap irradiation. Therefore, the detailed experimental results on Cu_2O will be described separately. First, we will focus our attention on the mechano-

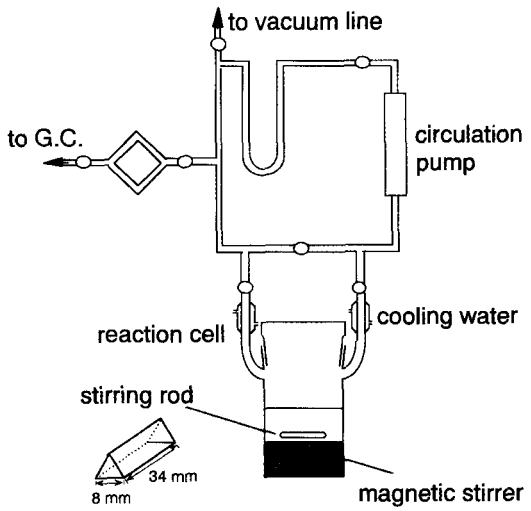

Fig. 24. A schematic view of apparatus. The reaction was carried out in a flat-bottomed reaction cell made of Pyrex® glass with 0.1 g of oxide powders and 200 cm^3 of distilled water which was magnetically stirred (F-205, Tokyo Garasu Kikai, stirring rate 1500 rpm, stirring rod triangular prism-type stirring rod ($8^3 \times 34$ mm) sealed by PTFE (Teflon®)) in most of the experiments. A closed gas circulation and evacuation system made of Pyrex® glass was connected to the reaction cell and evolved gases were accumulated in it (470 cm^3) for a gas chromatography analysis without any contamination from air.

catalytic reactions without any irradiation.

2.3(a). Mechano-Catalytic Activity of Simple Oxides.[39] The "mechano-catalytic" activities of simple oxides for overall water splitting are summarized in Table 8. All reactions were carried out for 24 h; the rates in Table 8 are the averaged values. NiO, Co_3O_4, Cu_2O, and Fe_3O_4 are seen to exhibit extreme activity. It should be noted that neither CuO, FeO, Fe_2O_3, nor CoO evolved H_2 and O_2 simultaneously although small amounts of H_2 were detected in the latter three. It was also confirmed that RuO_2 and IrO_2 had much lower activity for the stoichiometric evolution of H_2 and O_2. Cr_2O_3 also evolved both H_2 and O_2, but the amount of O_2 was much less than the stoichiometry. The cause of the lack of the concurrent evolution of H_2 and O_2 is not clear at present, but the redox reaction of the metal component may be responsible for such a behavior. On the other hand, TiO_2, ZnO, and WO_3 which are widely used as photocatalytic materials were completely inert.

2.3(b). Stoichiometric H_2 and O_2 Evolution on NiO.[39] Figure 25 shows typical time courses of H_2 and O_2 evolution on NiO. The reaction system was evacuated at 10—15 h intervals. Stoichiometric evolution of H_2 and O_2 was observed, while the rate of H_2 and O_2 evolution decreased with the accumulation of the evolved gas probably due to the effect of the gas phase pressure. A similar decrease of the activity was observed when Ar, H_2 or O_2 was introduced into the gas phase of the reaction system. The lack of dependence of supression on the kinds of gases excludes the possibility of the reverse reaction ($H_2 + 1/2O_2 \rightarrow H_2O$). Actually, no reverse reaction was observed when the NiO powder was

Table 8. Activity of Various Oxides to Overall Water Splitting ($\mu mol\ h^{-1}$)[a)]

Oxides	H_2	O_2
Cr_2O_3	1.0	0.001
MnO	0	0
Mn_3O_4	0	0.01
MnO_2	0	0
FeO	0.5	0
Fe_2O_3	0.02	0
Fe_3O_4	**1.68**	**0.97**
CoO	0.3	0
Co_3O_4	**44.2**	**22.5**
NiO	**46.0**	**22.7**
CuO	0	0
Cu_2O	**5.7**	**3.7**
ZnO	0	0
Sc_2O_3	0	0
MgO	0	0
Y_2O_3	0	0
TiO_2	0	0
ZrO_2	0	0
V_2O_5	0.06	0
Nb_2O_5	0	0
Ta_2O_5	0	0
MoO_3	0	0
WO_3	0	0
RuO_2	**0.1**	**0.05**
Rh_2O_3	0	0
IrO_2	**0.22**	**0.07**
PdO	0	0.2
Ag_2O	0	0
CdO	0.05	0
Al_2O_3	0	0
Ga_2O_3	0.04	0
In_2O_3	0	0
SiO_2	0	0
SnO_2	0	0
SnO	0.006	0
PbO	0	0
Pb_3O_4	0	0.1
PbO_2	0	0.3
Bi_2O_3	0	0.007
La_2O_3	0.1	0
CeO_2	0	0
Pr_5O_{11}	0	0
Nd_2O_3	0	0
Sm_2O_3	0	0
Dy_2O_3	0	0
Ho_2O_3	0	0
Er_2O_3	0	0
Tm_2O_3	0	0

Each reaction was continued for 24 h, and the total amounts of evolved H_2 and O_2 were divided by 24. a) All the reactions were carried out using a flat-bottomed reaction vessel with 0.1 g of oxide powders and 200 cm^3 of distilled water which was magnetically stirred. A triangular prism-type stirring rod ($8^3 \times 34$ mm) sealed by PTFE was used (see Fig. 24). Catalyst 0.1 g, H_2O 200 cm^3, Stirring rate 1500 rpm.

stirred in the presence of H_2 (20 kPa) and O_2 (20 kPa) in gas phase. Almost the same time courses were reproduced in the subsequent runs after evacuation of gas phase although

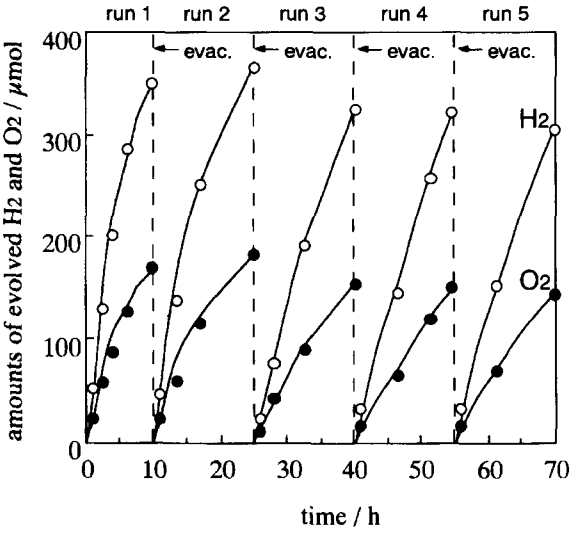

Fig. 25. Time course of H_2 (open circles) and O_2 (filled circles) evolution from NiO suspended in distilled water system. The gas phase was evacuated at 10 h after startup (Run 1) and at 15 h intervals in subsequent runs. The molar amount of evolved H_2 and O_2 after 5 runs reached to 1700 and 840 μmol, respectively. Catalyst (NiO): 0.1 g, H_2O: 200 cm^3, Stirring rate: 1500 rpm.

the rates of H_2 and O_2 evolution slightly decreased during the successive runs. It should be mentioned that the total amounts of evolved H_2 and O_2 reached to 1700 and 840 μmol after 5 runs, respectively, exceeding the amount of NiO used (1300 μmol, 0.1 g). Thus, the reaction is confirmed to proceed catalytically.

Similar time courses were also observed when Co_3O_4, Cu_2O, or Fe_3O_4 was used (results not shown). Inductively coupled plasma (ICP) and pH measurements of the aqueous solution showed that there was no appreciable dissolution of the oxides nor any change of pH in suspension during the reaction.

2.3(c). Mechano-Catalytic Overall Water Splitting on $CuMO_2$.[37,38] The observation shown in Table 9 suggests that the reaction proceeds on the oxides that contain some special elements in specific oxidation states. This well agrees with our finding that Cu(I) containing delafossites, $CuMO_2$ (M = Al, Ga, Fe), were also active for the reaction. Ternary Cu(I)-containing oxides of the general formula $Cu^{1+}M^{3+}O_2$

Table 9. Activity for Overall Water Splitting on Some Delafossite Oxides

$CuM(III)O_2$ (delafossite)	Rate of evolved gases ($\mu mol\ h^{-1}$)	
	H_2	O_2
$CuAlO_2$	10.95	5.10
$CuFeO_2$	3.08	1.56
$CuCrO_2$	0.07	0
$CuGaO_2$	13.36	6.89
$CuLaO_2$	0	0
$CuYO_2$	0.01	0
$CuEuO_2$	0.02	0

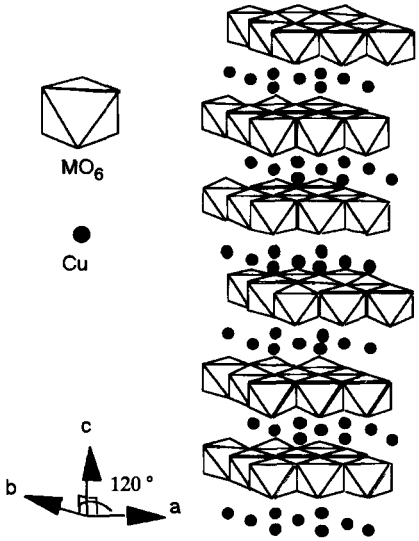

Fig. 26. Schematic structure of the delafossite oxides, $CuMO_2$. The structure belongs to the trigonal system with cell parameters a_h = 3.035 Å and c = 17.066 (i.e. $CuFeO_2$) in the hexagonal description.

are crystallized in the delafossite structure (Fig. 26).[42,43] The MO_6 octahedra share edges to form a triangular plane. The monovalent Cu ions are linearly coordinated with two oxygen ions on the surface of the MO_6 layer.

Figure 27 shows time courses of H_2 and O_2 evolution on $CuFeO_2$. During the first 20 h, the reaction (Run 1) was carried out under visible light irradiation (> 420 nm) and then the reaction (Run 2) was continued in dark for a subsequent 20 h after evacuation. H_2 and O_2 evolved in a stoichiometric ratio in both Runs 1 and 2, and there was no appreciable difference in activity between Runs 1 and 2. This confirms that there is no photo-irradiation effect on mechanocatalytic overall water splitting except Cu_2O. On the other hand, H_2 and O_2 evolution was not observed in Run 3 under visible light irradiation without stirring. It shows a typical dependence of H_2 and O_2 evolution on the stirring. More quantitative results will be shown below. The results indicate that the reaction occurs by stirring (mechanical effect), and that the light irradiation (photon energy) has no effect on the reaction.

To examine the effective component, the activity of overall water splitting on several Cu(I)-containing delafossite oxides was examined in dark condition as summarized in Table 9. Stoichiometric H_2 and O_2 evolution was observed on $CuFeO_2$, $CuGaO_2$, and $CuAlO_2$, while the other delafossite oxides did not exhibit any activity. As shown in Table 9, Cu_2O is an active material for the reaction, while CuO did not show any activity. Fe_2O_3, Ga_2O_3, and Al_2O_3 are also inert materials. Cu(I) is, therefore, essential for the reaction on these delafossite oxides. As shown in Table 9, however, M(III) cations in the octahedral plane also influence the activity. This result might give some clue to understand the overall mechanism of mechano-catalytic water splitting.

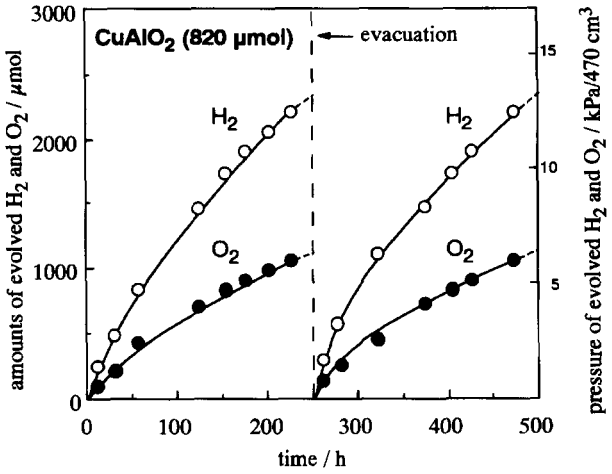

Fig. 28. Time course of H_2 (open circles) and O_2 (filled circles) evolution for the $CuAlO_2$ suspension. The gas phase was evacuated at 250 h after startup. The molar amount of evolved H_2 and O_2 (about 5000 and 2500 μmol, respectively) exceeded the amount of the used $CuAlO_2$ (820 μmol). Catalyst ($CuAlO_2$); 0.1 g, H_2O; 200 cm^3.

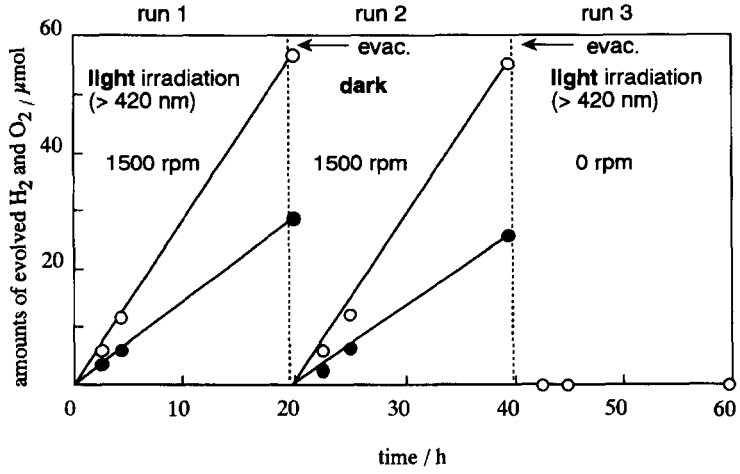

Fig. 27. Time courses of H_2 and O_2 evolution on $CuFeO_2$ under visible light (> 420 nm) irradiation and in dark. The closed-gas circulation system was evacuated at ca. every 20 h. The rotation rates of the stirring rod were 1500 rpm in Runs 1 and 2, and 0 rpm in Run 3. Catalyst; 0.1 g, H_2O; 200 cm^3, light source; Xe lamp (300 W).

Figure 28 shows typical time courses of H_2 and O_2 evolution on $CuAlO_2$ catalyst (0.1 g = 820 μmol was used). The reaction was continued for about 500 h with an intermediate evacuation at ca. 250 h. The observed time course resembled that observed on NiO (see Fig. 25), and it was again confirmed that the molar amounts of the evolved H_2 and O_2 after the reaction for 500 h definitely exceeded the amount of the used $CuAlO_2$.

2.3(d). Mechanical Energy Responsible for the Reaction.[39] Figure 29 shows the relationship between the revolution rate (rpm) of the stirring rod and the rates of H_2 and O_2 evolution on NiO. H_2 and O_2 evolution was not observed without stirring (0 rpm) as mentioned above. The stirring rod was rotated without any supply of such energies as light or heat but the rates of H_2 and O_2 evolution increased monotonically with the revolution rate. It is again confirms that the reaction proceeded with the mechanical energy exerted by the stirring rod.

The role of magnetic field was examined by an experiment in which an electric motor was used to rotate a stirring rod made of alumina (10 mm of radius), while 0.01 g of NiO powder was attached to the flat bottom of it. Then the stirring rod that was pressed to the bottom of the reaction cell. As shown in Fig. 30, simultaneous evolution of H_2 and O_2 was observed, further supporting the conclusion that the magnetic field is not responsible for the mechano-catalytic reaction. Similar results were obtained also for other active oxides.

Mechanical energy injected into the reaction system via stirring may be classified into the energy consumed for stirring the aqueous suspension, and the energy deposited by scrapping at the interface between the rotating stirring rod and the bottom wall of the reaction vessel. In order to determine which mechanical energy leads to the mechano-catalytic reaction, the relationship between the reaction and the stirring manner was examined by using differently-shaped

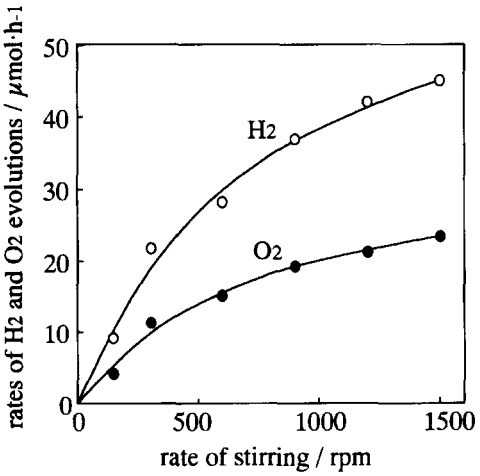

Fig. 29. The rates of H_2 (open circles) and O_2 (filled circles) evolution for the NiO-suspended system as a function of the revolution rate (rpm) of the stirring rod. The rates of H_2 and O_2 evolution monotonously increased with increasing the revolution rates of the stirring rod. Catalyst (NiO); 0.1 g, H_2O; 200 cm^3.

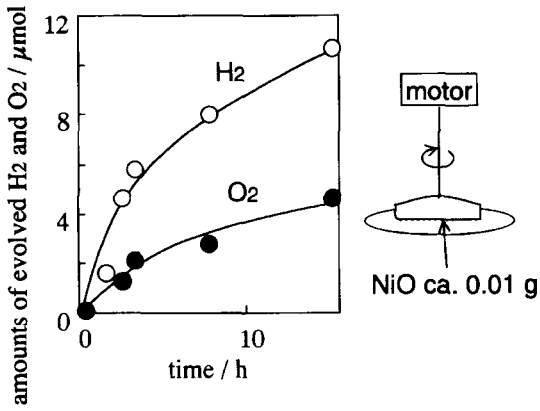

Fig. 30. Time courses of H_2 and O_2 evolution in the reaction performed under free-of-magnetic-field condition. Schematic view of motor-drive type reaction cell is shown by inset. 0.01 g of NiO powder was stuck onto the flat bottom of the stirring rod made of alumina. A simultaneous H_2 and O_2 evolution was observed. H_2O; 200 cm^3, stirring rate; 1500 rpm.

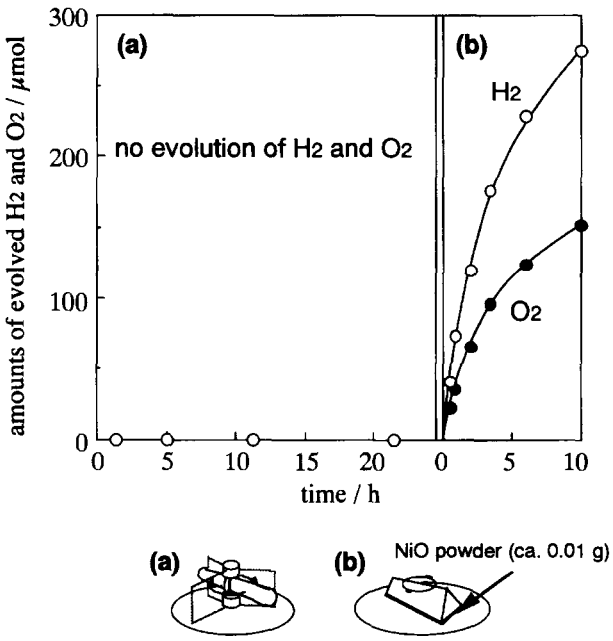

Fig. 31. Change by stirring manner of the rates of H_2 (open circles) and O_2 (filled circles) evolution. (a) Stirring NiO (0.1 g)-suspended distilled water with a floating type stirring rod, the stirring rod was rotated without contact with the bottom of the reaction vessel. There was no evolution of H_2 and O_2. (b) Both-sided adhesive tape was stuck on the flat bottom of the stirring rod and ca. 0.01 g of NiO powder was stuck onto the other side of the tape. Stirring the NiO (ca. 0.01 g)-glued flat-bottomed rod in suspension-free water. Similar to the suspension system shown in Fig. 24, A simultaneous H_2 and O_2 evolution was observed. H_2O; 200 cm^3, stirring rate; 1500 rpm.

stirring rods. The shapes of the two tested stirring rods and the time courses of H_2 and O_2 evolution are depicted in Fig. 31. In the first experiment, 0.1 g of NiO powder was suspended in distilled water by rotating the stirring rod (a) that

was kept from contact with the bottom wall of the reaction vessel. There was no evolution of H_2 and O_2 (Fig. 31(a)). In the second experiment, ca. 0.01 g of NiO was stuck by a double-sided adhesive tape onto the bottom face of the stirring rod (b) with a flat bottom, and the rod was rotated on the bottom of the reaction vessel in distilled water in the absence of any suspended NiO powders (Fig. 31(b)). Similarly to the suspension system shown in Fig. 25, a stoichiometric evolution of H_2 and O_2 was observed in this case. These results proved that the reaction was driven by the mechanical energy consumed at the interface between the rotating stirring rod and the bottom of the reaction vessel. Moreover, it is indicated that the collisions among the oxide particles or at the stirrer surface do not influence the reaction. Additionally, the result also excluded the possibility of the participation of the Teflon® film coating the stirring rod in the reaction, because no Teflon® but adhesive tape contacted with NiO powder and the bottom of the reaction vessel in the second experiment. As a whole, the simultaneous H_2 and O_2 evolution on these oxides is the "mechano-catalytic" overall water splitting in which mechanical energy supplied by the "rubbing" of these oxide powders on the bottom of reaction vessel is converted to chemical energy with a help of these oxide powders as a catalytic material.

2.3(e). Efficiency of Mechanical-to-Chemical Energy Conversion.[39] Estimation of the efficiency of mechanical-to-chemical energy conversion was carried out as follows. We denote by E_c, E_t, E_i, and η the chemical energy accumulated for an hour by water decomposition, the total mechanical energy provided into the system for an hour for stirring, the mechanical energy consumed at the interface for an hour between the rotating rod and the bottom of the reaction vessel, and conversion efficiency from E_i to E_c, respectively, and express E_c, E_t, and E_i in the unit of kJ h^{-1}. E_c was obtained from the measured rate of water decomposition. The estimation of E_t and E_i was made as follows. The stirring rod mounted at the end of a driving shaft was rotated by an electric motor to stir the suspension (catalyst: 0.1 g, H_2O: 200 cm^3) in the reaction vessel (see Fig. 32). The stirring rod was pressed against the bottom wall of the reaction vessel with the force of 1.9 N, which was the same as that being exerted by a magnetic stirrer. E_t was then derived by measuring the torque and the rate of revolution according to the following equation:

$$E_t(\text{kJ h}^{-1}) = 2\pi \times (\text{revolution rate (rpm)}/60\ (s)) \times \text{torque (N m)} \times 3600\ (s). \quad (2)$$

E_i, which is the mechanical energy responsible for the reaction, was obtained by subtracting from E_t the energy, $E_{t'}$, derived by releasing the pressing force of 1.9 N (i.e. $E_i = E_t$ (under rubbing) $-E_{t'}$ (without rubbing)). The energy for such free stirring of suspension was determined by measuring the torque when the stirring rod was rotated in the suspension without touching the bottom of the reaction vessel. Conversion efficiency, η, was then obtained by the following equation:

$$\eta(\%) = E_c/E_i \times 100. \quad (3)$$

According to the definition and the method described above, E_c and E_i were estimated as follows when using the data of NiO described in Table 8.

$$E_c = 46\ \mu\text{mol h}^{-1} = 0.011\ \text{kJ h}^{-1}, \quad (4)$$

$$E_i = 0.83\ \text{kJ h}^{-1}, \quad (5)$$

$$\eta = 0.011/0.83 \times 100 = 1.3\ (\%). \quad (6)$$

When a larger stirring rod with triangular prism-shape (133×54 mm) was used for NiO catalyst, higher efficiency was obtained as follows:

$$E_c = 200\ \mu\text{mol h}^{-1} = 0.047\ \text{kJ h}^{-1} \quad (7)$$

$$E_i = 1.10\ \text{kJ h}^{-1} \quad (8)$$

$$\eta = 0.047/1.10 \times 100 = 4.3\ (\%). \quad (9)$$

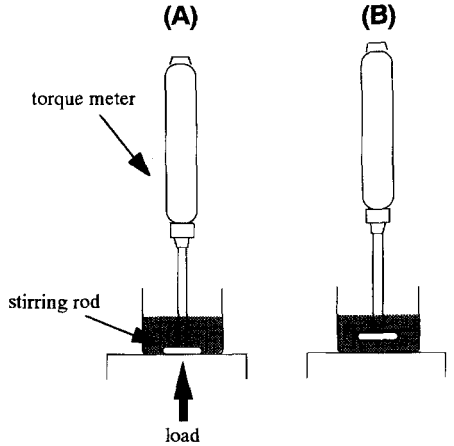

Fig. 32. Schematic views of the apparatus used for estimation of the efficiency of mechanical-to-chemical energy conversion; (A) for Et (under rubbing) and (B) for Et′ (without rubbing), see text.

2.3(f). The Effect of Aqueous Solution.[39] So far, H_2 and O_2 evolution from distilled water has been described. The effect of the reaction solution was next examined to obtain information on the reaction mechanism. It is well known that O_2 evolution is completely suppressed in an aqueous methanol solution in the case of photocatalytic decomposition of water, because the intermediate species of water oxidation, i.e. OH· radicals and/or O^- ions, preferentially attack methanol molecules which are oxidized eventually into CO_2 molecules. Figure 33 shows a time course of H_2 and O_2 evolution on NiO from an aqueous methanol solution (10 vol%). In contrast to the conventional photocatalytic reactions, both H_2 and O_2 were evolved in the present system, although the amount of O_2 was slightly less than the stoichiometry. The result suggests that the formation of O_2 molecules by mechano-catalysis does not proceed through these intermediate species formed in a bulk of aqueous solution.

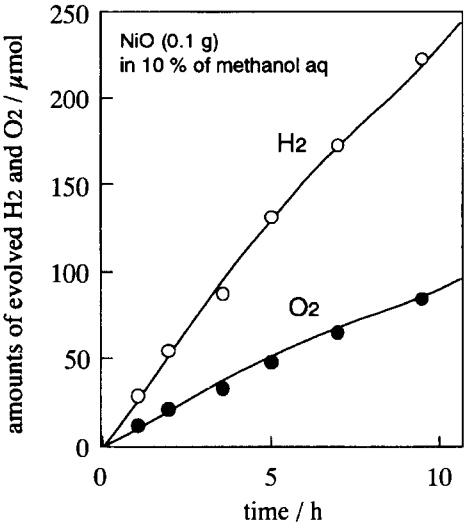

Fig. 33. Time courses of H_2 (open circles) and O_2 (filled circles) evolution from the NiO-suspended aqueous methanol solution. Catalyst (NiO); 0.1 g, 10% methanol aq; 200 cm^3, Stirring rate; 1500 rpm.

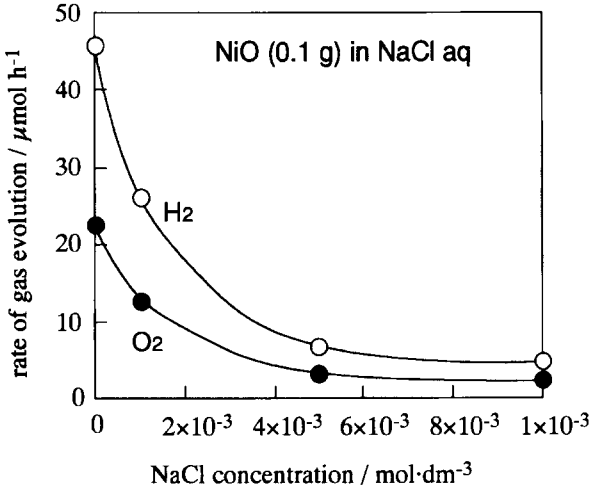

Fig. 34. Dependence on the concentration of NaCl of the rates of H_2 (open circles) and O_2 (filled circles) evolution in the NiO–water system. Catalyst (NiO); 0.1 g, H_2O; 200 cm^3, Stirring rate; 1500 rpm.

To examine the contribution of electrolytes in the aqueous solution, the reaction in the presence of some electrolytes was carried out. Figure 34 shows a typical dependence of the mechano-catalytic activity of NiO on the concentration of NaCl in the reaction mixture. The rates of H_2 and O_2 evolutions monotonously decreased with increasing the concentration of NaCl. Similar results were observed in the presence of other electrolytes such as Na_2SO_4, $NaNO_3$, and KCl as listed in Table 10, and also on Co_3O_4, Cu_2O, and Fe_3O_4. These results indicate that the addition of any electrolyte to the aqueous solution retards the rate of mechano-catalytic overall water splitting.

2.3(g). Materials of the Bottom of the Reaction Vessel.[39] From the experimental results described above, it has become clear that the rubbing of powder of the mechano-catalyst onto the bottom of the reaction vessel is essential. All the data presented so far were obtained in reaction vessels of Pyrex® glass. The reaction was also examined by employing other materials at the bottom of the reaction vessel, as shown in Table 11. In the case of a quartz glass plate, stoichiometric evolution of H_2 and O_2 was observed but the rate of the reaction was about a half of the case using a Pyrex® glass plate. When Al_2O_3 (sapphire) and CaF_2 plates were used, H_2 and O_2 evolutions were again confirmed although the rates decreased by more than an order of magnitude. The use of PTFE or acrylate board resulted in detecting a small amount of H_2 but no O_2 after the reaction for 20 h.

Table 10. Dependence of the Activity for Overall Water Splitting upon Kinds of Electrolytes in H_2O

Electrolyte	Concn	Rate of evolved gases (μmol h^{-1})[a]		pH	Conductivity (25 °C, *18 °C)
	mol dm^{-3}	H_2	O_2		(Ω^{-1} cm^{-1})
None	—	42.0	21.0	6.8	$<1\times10^{-5}$
NaCl	0.001	26.1	13.2	6.8	7.2×10^{-3}
	0.05	6.6	3.2	6.8	3.5×10^{-2}
	0.01	4.1	1.7	6.8	6.9×10^{-2}
$NaNO_3$	0.001	21.8	13.2	6.8	1.0×10^{-2}
Na_2SO_4	0.0005	21.2	11.9	6.2	7.2×10^{-3} *
	0.001	13.7	5.9	6.0	1.4×10^{-2} *
KCl	0.001	18.1	8.6	6.8	1.1×10^{-2}
KNO_3	0.001	16.4	10.0	6.8	1.4×10^{-2}
NaOH	0.001	5.2	2.4	11.0	8.6×10^{-3} *
KOH	0.001	3.2	1.2	11.0	1.3×10^{-2} *
HCl	0.001	7.6	1.6	3.0	1.5×10^{-2}
H_2SO_4	0.0005	7.0	3.8	2.9	2.0×10^{-2}

NiO 0.1 g, H_2O 200 cm^3, stirring rate 1500 rpm, a) Initial activity.

2.3(h). Formation of Metallic Elements During Mechano-Catalytic Overall Water Splitting.[41] Figure 35 shows the XRD patterns of Cu_2O before (A) and after (B) the reaction for 150 h. A small peak due to metallic copper (Cu(111) diffraction) appeared after the reaction; it was absent before the reaction. The peak was observed even after the reaction for 10 h, and remained unchanged after 20 h. It is found that Nafion®-coating enhances the activity of mechano-catalytic overall water splitting of Cu_2O although the mechanism of the enhancement is not yet clear.[40] The

Table 11. Dependence of the Activity for Overall Water Splitting upon the Quality of the Materials at the Bottom of the Reaction Vessel

Plate	Rate of evolved gases (μmol h^{-1})	
	H_2	O_2
Quartz glass	19	10
Pyrex® glass	40	20
Sapphire	0.9	0.5
CaF_2	0.8	0.3
PTFE	1.0	—
Acryl	0.8	—
Pyrex® frosted glass	6	3

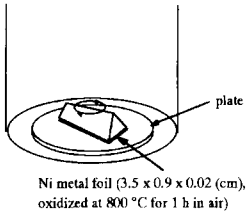

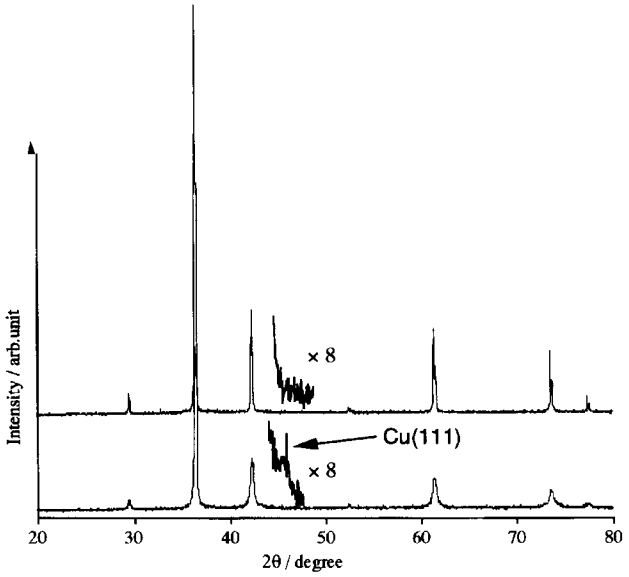

Fig. 35. XRD patterns of Cu_2O before and after the reaction for 160 h. A: Cu_2O before reaction and B: Cu_2O after reaction.

XRD pattern of Nafion®/Cu_2O before the reaction was the same as that of the original Cu_2O, while that after the reaction (not shown) exhibited a larger peak of metallic Cu than that in Fig. 35(B). When Cu_2O and Nafion®/Cu_2O were kept in distilled water for 500 h without stirring, no evolution of H_2 and O_2 together with the absence of the peak of metallic Cu was observed for Cu_2O and Nafion®/Cu_2O. Considering the fact that the peak of metallic Cu in Nafion®/Cu_2O was larger than that in Cu_2O, and that Nafion®/Cu_2O has a higher activity for water splitting, one may conclude that the formation of metallic Cu is related with the mechanism of the mechano-catalytic overall water splitting.

After the mechano-catalytic reaction over NiO or Co_3O_4 for 50 h, no metallic Ni or Co was observed by XPS or XRD. As the redox potentials of Ni and Co are more positive than Cu, metallic Ni and Co may be reoxidized by water immediately after the formation. KI–I_2 solution was used to clarify whether NiO and Co_3O_4 are reduced into metals during the reaction or not, which is often utilized for the detection of metals in metal oxides. I_2 in KI–I_2 solution oxidizes a transition metal denoted as M such as Ni and Co as follows:

$$M + I_2 \longrightarrow MI_2 \quad (10)$$

Even in KI–I_2 solution, both H_2 and O_2 evolution was observed, although the ratio was not stoichiometric. The deviation from the stoichiometry was attributed to the reduction of I_2. The decrease of I_2 was estimated by UV-visible absorption spectroscopy, and it coincided well with the shortage of the evolved H_2. Furthermore, the amounts of dissolved Ni^{2+} and Co^{2+} agreed with those expected from the decrease of I_2. It is noted that without I_2 no dissolution of Ni or Co was detected, and even metallic Ni or Co was formed under H_2 atmosphere. These experiments therefore indicated that metallic Ni and Co were formed during the mechano-catalytic overall water splitting on NiO and Co_3O_4. Thus, the formation of metallic elements in mechanocatalysts during the reaction seems to be a common phenomenon at least for the three oxides examined. This, however, does not necessarily mean that metals themselves directly participate in the reaction because the metals might be formed as by-product. The role of metals in the reaction was examined by the reaction of water with metallic Cu, Ni, and Co. For example, 0.11 g of CuO powder (1.4 mmol) was reduced at 423 K for 24 h by H_2 in the reaction vessel. The particle size and surface area of metallic Cu were estimated to be 6 μm and 1.0 $m^2\,g^{-1}$ by SEM (scanning electron microscopy) and BET measurements. 120 cm^3 of distilled water that was free from air was introduced into the reaction vessel, and then the solution was magnetically stirred. Only H_2 was evolved at the early stage of the reaction, but O_2 evolution became observable after the reaction for 30 h. The evolution rate of H_2 increased with the beginning of O_2 evolution, and the ratio of evolution rates of H_2 to O_2 (H_2/O_2) approached to 2 : 1 with reaction time. The XPS spectra and XRD patterns showed that the surface of metallic Cu is oxidized into Cu_2O during the reaction. These results indicate that metallic Cu was oxidized into Cu_2O by reducing water into H_2 at the early stage of the reaction where only H_2 was evolved. When the surface of Cu particles was covered with some amount of Cu_2O, O_2 began to evolve with H_2. In the cases of Ni and Co, we obtained similar results. From these results, it was concluded that metallic Cu, Ni, and Co were oxidized into Cu_2O, NiO, and Co_3O_4, respectively, by reducing water into H_2; the stoichiometric evolution of H_2 and O_2 was achieved when these metals were covered with the metal oxides.

2.3(i). Change of Particle Sizes of Catalysts.[40] Destruction of particles is one of the important causes in the cases of mechanochemical or tribochemical reactions. Because mechano-catalytic overall water splitting proceeds by rubbing the catalysts, the effect of the change of catalyst in particle size by grinding should be examined. Particle sizes and surface areas of Cu_2O, Nafion®/Cu_2O, NiO and Co_3O_4 before and after the reaction for 24 h were examined. These were estimated by SEM and BET measurements, respectively. Each particle was ground to the smaller one during the reaction for 24 h, while the particles were not further ground during the subsequent reaction for 100 h, indicating that the grinding of the metal oxide particles is completed at the very early stage of the reaction. Therefore, the grinding is not directly related to the reaction because the rates of H_2 and O_2 evolution on the metal oxides were stable for more than 100 h.

2.3(j). The Origin of Evolved O_2.[39] The origin of evolved O_2 was confirmed by using $H_2{}^{16}O/H_2{}^{18}O$ mixture. The reaction was carried out with 0.01 g of $CuAlO_2$ and a mixture of $H_2{}^{16}O$ and $H_2{}^{18}O$ ($H_2{}^{16}O/H_2{}^{18}O = 4.7$), which was magnetically stirred. After the stoichiometric H_2 and O_2 evolution was confirmed by gas chromatography, the evolved O_2 species were analyzed by mass spectral analysis. Figure 36 shows a time course of isotope composition in evolved O_2 on $CuAlO_2$ from $H_2{}^{16}O/H_2{}^{18}O$ mixture. At the beginning

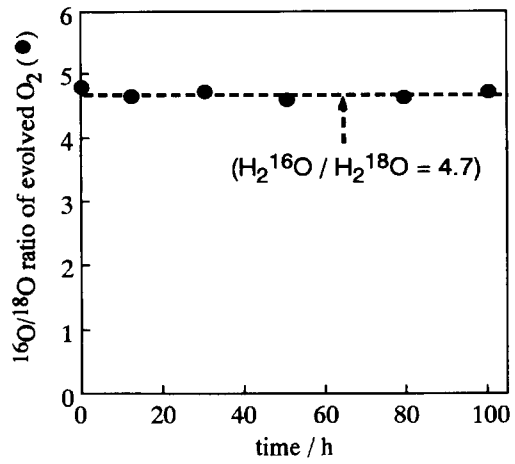

Fig. 36. Time courses of isotope composition of the O_2 (filled circles) evolved from the NiO-suspended $H_2{}^{16}O/H_2{}^{18}O$ mixture. Catalyst (NiO); 0.01 g, H_2O ($H_2{}^{16}O/H_2{}^{18}O = 4.7$); 4 cm^3, Stirring rate; 1500 rpm.

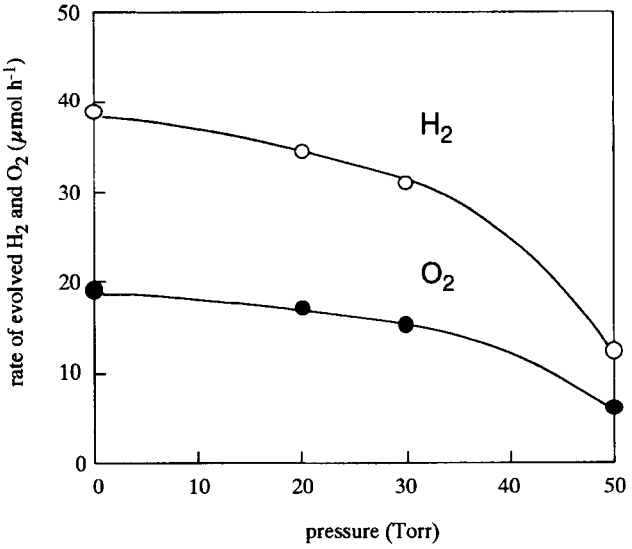

Fig. 37. Dependence of the activity for overall water splitting upon Ar pressure in gas phase; NiO; 0.1 g, H_2O; 200 cm^3, stirring rate; 1500 rpm.

stage of the reaction for 1 h, the ratio, $^{16}O_2/^{16}O^{18}O/^{18}O_2$, in the evolved O_2 was estimated to be 22.0/9.5/1.0. Therefore, the atomic ratio, $^{16}O/^{18}O$, in the total amount of evolved O_2 is 4.7/1.0, which exactly coincided with that in the water. The $^{16}O/^{18}O$ ratio did not change in subsequent measurements up to 76 h. The same results were also obtained on NiO, Co_3O_4, Cu_2O, and Fe_3O_4.

2.3(k). The Effect of Gas Pressure of the System.[44] The rate of evolution of H_2 and O_2 gradually decreased in the time course of the mechano-catalytic water decomposition regardless of the type of catalyst (Figs. 25, 28, 30, 31, and 33). This is not due to the deactivation of the catalyst because the initial activity was recovered by evacuation. The increase of the gaseous pressure was found to be responsible for the decrease of the reaction. The mechano-catalytic water decomposition was observed on NiO with various Ar pressures, and the rate of evolution of H_2 and O_2 was plotted as a function of the Ar pressure in Fig. 37. It has become clear that the increase of Ar pressure suppresses the rate of gas evolution. An interesting result was obtained by changing the kind of gas in the system. The same pressures (50 or 20 Torr, 1 Torr = 133.322 Pa) of Ar and O_2, or Ar, O_2, and H_2 resulted in the same rates of gas evolution, as demonstrated in Fig. 38. The pressure dependence on the suppression was also confirmed by O_2. The lack of any specific dependence on H_2 or O_2 indicates that the reverse reaction is not responsible. The absence of the reverse reaction was practically confirmed by an experiment: When NiO powders were stirred in a reaction cell without water but under H_2 and O_2 gases, no decrease of the pressure was observed.

The pressure in gas phase is considered to influence on the decrease of the rate of diffusion of the generated H_2 and O_2 in water to gas phase. The increase of the residence time of O_2 in water by increasing the gaseous pressure may cause readsoreption of O_2 molecules, which results in the suppression of the reaction.

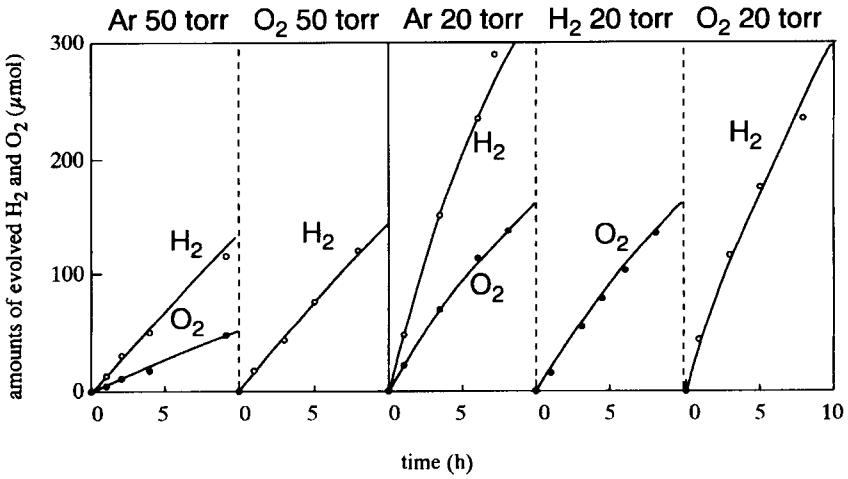

Fig. 38. Dependence of the activity over NiO catalyst as a function of gas phase pressure and kinds of gases; NiO; 0.1 g, H_2O; 200 cm^3, stirring rate; 1500 rpm.

2.4. The Mechanism of Mechano-Catalytic Overall Water Splitting. 2.4(a). Non Thermal Mechano-Catalysis. The standard Gibbs free energy change, ΔG°, of overall water splitting is as large as 237 kJ mol^{-1} for liquid water at 298 K. It is 229 (298 K), 193 (1000 K) or 135 (2000 K) kJ mol^{-1} in gas phase. This indicates that the equilibrium pressures of H_2 with H_2O(g) of 1 bar are 3×10^{-27} and 5×10^{-4} bar at 298 and 2000 K, respectively. In the present study, more than 0.1 bar of H_2 was accumulated under 0.04 bar of the vapor pressure of H_2O at 298 K (see Fig. 26). Although the increase in temperature at the interface between a rotating stirring rod and the bottom of the reaction vessel is expected to some extent, any temperature above 2000 K is extremely unlikely. It is, therefore, obviously concluded that the H_2 and O_2 evolution is not due to thermally driven reaction. Some other process than heat of friction should be considered for the mechano-catalytic overall water splitting. In mechanochemistry, as a matter of fact, some reactions with $\Delta G > 0$ (e.g. $Au + 3/4CO_2 \rightarrow 1/2Au_2O_3 + 3/4C$, $\Delta G^\circ = 377$ kJ mol^{-1}) are known to proceed by using mechanical energy.[45,46] The activation processes of these reactions are generally attributed to the grinding or frictional wear of materials: The reactions are classified into stoichiometric and irreversible reactions. As mentioned above, in the cases of NiO, Cu_2O, Co_3O_4, and Fe_3O_4, the particle sizes of those oxides became smaller at the beginning stage of the reaction but they were almost unchanged after the period, while the reaction proceeded steadily for long time. There results indicate that the grinding or frictional wear is not really essential for the mechano-catalytic overall water splitting. The "mechano-catalytic" overall water splitting is one of the *catalytic* reactions, which are different from the mechanochemical, and/or tribochemical reactions, and the molar amounts of evolved H_2 and O_2 far exceeds that of the catalysts.

2.4(b). Redox Mechanism.[41] Reversible mechanical effects without any wear of the materials have to be considered for interpreting the reaction mechanism of the mechano-catalytic overall water splitting. One of the possible explanations is the so-called "triboelectricity", although the origin of this phenomenon does not seem to be fully understood even now. It is known that electrostatic charge separation can take place easily in vacuum or under gas phase condition when two materials are frictionally contacted. As a result, the oxide powder may be negatively charged, and the bottom of the reaction vessel may be positively charged. These triboelectrically generated charges may be able to cause the redox reactions resulting in overall water splitting. In our preliminary experiments, photoemission was actually observed from the interface where the stirring rod is rotating. This may suggest that such electrostatic charge separation can take place even in an aqueous solution. As mentioned in the preceding section, the rate of H_2 and O_2 evolution decreased when some electrolytes were added into distilled water. This seems to indicate that the charge separation at the interface becomes more difficult in an aqueous solution containing electrolytes. Although at present the triboelectricity is a most probable candidate for the first step of the mechano-catalytic overall water splitting, there are several experimental results that seem to be opposing to this model and have to be explained. First, no evolution of H_2 and O_2 was observed when we carried out the reaction in water vapor. Gas phase reaction seems to be more facile for the triboelectric charge separation. Second, if triboelectricity is responsible for the mechanocatalysis, the efficiency of conversion from mechanical-to-chemical energy seems to be very high. As shown above, the estimated value was as high as 4.3%. As we do not know how the maximum efficiency of triboelectricity is estimated, this value might be reasonable. Then, another question as to what is the ultimate efficiency of this reaction will be raised. Third, only a limited number of oxides can efficiently decompose water into H_2 and O_2 and most oxides are inert. If charge separation is essential for the reaction, various kinds of materials, especially insulating ones such as MgO, Al_2O_3, and ZrO_2 are expected to be active. This suggests that there is another essential role of the oxide powders for the accomplishment of the overall water splitting by the mechano-catalysis.

The fact that only a few oxides with some specific oxidation states are active for the reaction suggests that these materials have some kind of catalytic activity of overall water splitting which is driven by the triboelectricity. As shown in Table 8, Fe_3O_4, Co_3O_4, NiO, Cu_2O, RuO_2, and IrO_2 evolved H_2 and O_2 in a stoichiometric ratio. Some of them (Co_3O_4, RuO_2, and IrO_2) are known to be good catalysts for O_2 evolution in water oxidation but Cu_2O and Fe_3O_4 seems to be not so effective. Co_3O_4, NiO, RuO_2, and IrO_2 are expected to work as good catalysts for water reduction to form H_2, but again Fe_3O_4 and Cu_2O are not. Therefore, a simple explanation from the viewpoint of catalytic activities for water oxidation and reduction seems not to be suitable. Furthermore, O_2 evolution from a methanol aqueous solution indicates that at least the water oxidation process does not proceed through the reaction mechanism similar to the photocatalytic oxidation of water. One of the possible reaction mechanisms for H_2 and O_2 evolution is based on the redox reaction of the oxide materials themselves.

The formations of metallic Cu, Ni, and Co were indicated during the mechano-catalytic reaction on Cu_2O, NiO, and Co_3O_4, as mentioned in Section 2.3(h). When the metallic Cu, Ni, and Co were used under the condition of mechano-catalytic reaction, H_2 evolution was also confirmed. Therefore, it is possible to reduce water into H_2 if the oxides are reduced to the metallic states, although the reduction mechanism of the oxides is unclear.

The experiments in KI–I_2 solution also indicated that NiO and Co_3O_4 were also reduced into metallic Ni and Co, respectively. In the reaction of water with metallic powders, metals were oxidized into the metal oxides by reducing water into H_2. Taking these results into consideration, we expect the metals formed in the metal oxides during mechano-catalysis to participate in the catalytic reaction cycle for overall water splitting. Therefore, we tentatively propose a redox model for the reaction mechanism of mechano-catalytic over-

all water splitting. Based on this assumption, thermodynamic aspects of the overall water splitting reaction are examined. Standard Gibbs free energy changes, ΔG°, at 298 K for water reduction by elemental metals are as follows:

$$3/4Co + H_2O \rightarrow 1/4Co_3O_4 + H_2 \qquad \Delta G^\circ = 45\ kJ\ mol^{-1} \quad (11)$$

$$Ni + H_2O \rightarrow NiO + H_2 \qquad \Delta G^\circ = 25\ kJ\ mol^{-1} \quad (12)$$

$$2Cu + H_2O \rightarrow Cu_2O + H_2 \qquad \Delta G^\circ = 89\ kJ\ mol^{-1} \quad (13)$$

On the other hand, standard free energy changes at 298 K for metal oxide reduction accompanied by O_2 formation are as follows:

$$1/4Co_3O_4 \rightarrow 3/4Co + 1/2O_2 \qquad \Delta G^\circ = 192\ kJ\ mol^{-1} \quad (14)$$

$$NiO \rightarrow Ni + 1/2O_2 \qquad \Delta G^\circ = 212\ kJ\ mol^{-1} \quad (15)$$

$$Cu_2O \rightarrow 2Cu + 1/2O_2 \qquad \Delta G^\circ = 148\ kJ\ mol^{-1} \quad (16)$$

As the standard free energy change for overall water splitting at 298 K is 237 kJ mol^{-1}, the redox mechanism divides the increment of the free energy into two steps as shown in the above equations and as shown also in Fig. 39. Of course, the energies for both steps are provided by mechanical energy consumed at the interface. Although both steps are so-called uphill reactions, water reduction steps, (11)—(13), are relatively facile. The existence of these steps was experimentally confirmed in this study. On the other hand, the reduction steps of metal oxides, (14)—(16), are accompanied by large increases of free energies. The formation of metallic species during mechano-catalysis in distilled water was substantiated in the present work. Judging from the equations (14)—(16), we think these reactions should proceed without water and even in vacuo. However, we were not able to observe any O_2 evolution in vacuo or even in water vapor using attached metal-oxide powders on the bottom of a stirring rod. This fact may suggest a more complicated process for O_2 formation than the simple reactions (14)—(16).

Another point worth noting in considering the reaction mechanism is the results obtained by the experiments using $H_2{}^{18}O$ as shown in Fig. 36.[39] The ratio of the isotopes of $^{18}O/^{16}O$ in evolved O_2 coincided with that in water. One of the interpretations of this result is that no oxygen in the oxide is incorporated in the catalytic cycle of water splitting. Another possibility is that, although the redox reaction of the oxide is responsible for the water splitting, the amount of oxygen of the oxide which is incorporated in the reaction is very small so that the ratio of the isotopes appears to be the same as that of water. If some of the oxygen in the oxide and that in water exchange very quickly under the mechano-catalytic condition, and only such oxygen atoms are incorporated in the redox reaction, then we again obtain the same isotope ratio.

As a whole, the experimental results in this work indicate the possibility of the redox mechanism for mechano-catalytic overall water splitting, but there exist several facts to be accounted for before the model is accepted. The proposed reaction scheme is only for "exit" of mechanical energy and does not explain the overall reaction including conversion process of mechanical energy into the redox reaction. In the field of mechanochemistry or tribochemistry, many reactions are known to proceed by mechanical energy.[47,48] As mechano-catalytic overall water splitting also proceeds by mechanical energy, reaction mechanisms proposed in mechanochemistry may be applicable to the catalytic reaction. One of the possible explanations of this phenomenon is "electrostatic

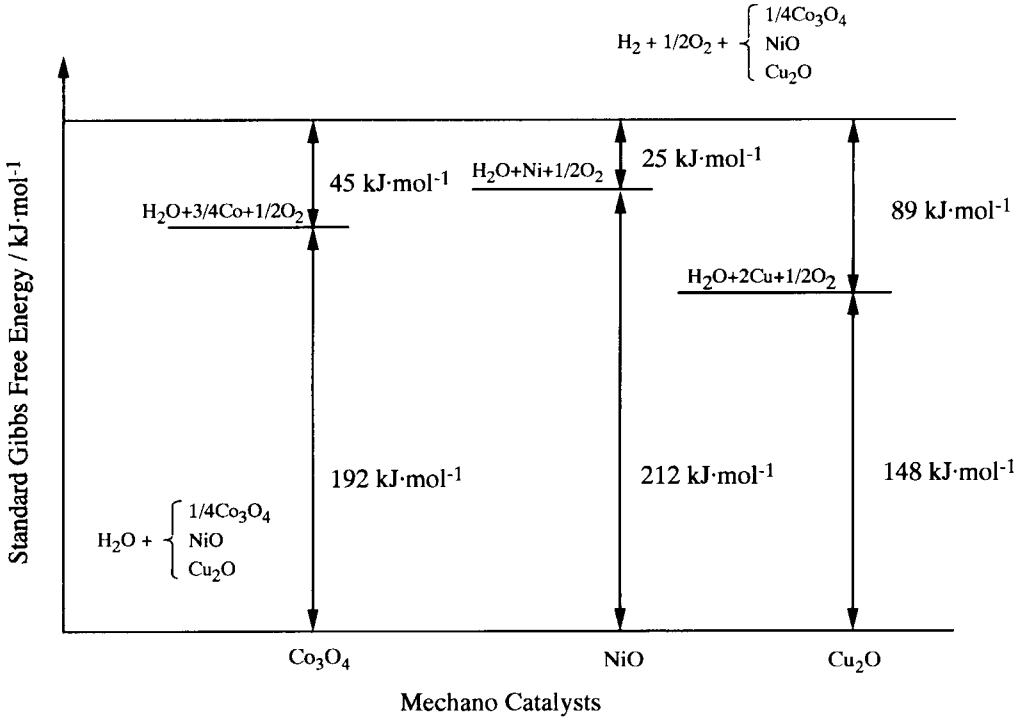

Fig. 39. Standard Gibbs free energy change of the redox model for mechano-catalytic overall water splitting.

charge separation" or "triboelectricity" due to frictional motion between two different materials, i.e. a catalyst powder and glass of a reaction vessel. From this point of view, we carried out several experiments and discussed on the mechanism as reported in our previous paper.[39,41] However, as has been discussed, the overall reaction mechanism seems to be more complicated in spite of the apparent simplicity of the reaction.

It is an important and interesting subject to reveal the reaction mechanism of this novel water splitting reaction not only from a fundamental point of view but also from the point of applications. It may provide a way to estimate the maximum efficiency of this reaction and a way to improve the efficiency. Therefore, further study on the reaction mechanism is now proceeding in our laboratory.

References

1 M. A. Grätzel, "Energy Resources through Photochemistry and Catalysis," Academic Press, New York (1983), and references therein.

2 K. Domen, A. Kudo, and T. Onishi, *J. Phys. Chem.*, **90**, 292 (1986).

3 K. Domen, A. Kudo, and T. Onishi, *J. Catal.*, **102**, 92 (1986).

4 A. Kudo, A. Tanaka, K. Domen, and T. Onishi, *J. Catal.*, **111**, 296 (1988).

5 N. Kinomura, N. Kumada, and F. Muto, *J. Chem. Soc., Dalton Trans.*, **1985**, 2349.

6 T. Takata, Y. Furumi, K. Shinohara, A. Tanaka, M. Hara, J. N. Kondo, and K. Domen, *Chem. Mater.*, **9**, 1063 (1997).

7 T. Takata, K. Shinohara, A. Tanaka, M. Hara, J. N. Kondo, and K. Domen, *J. Photochem. Photobiol., A: Chem.*, **106**, 45 (1997).

8 S. Ikeda, A. Tanaka, K. Shinohara, J. N. Kondo, K. Maruya, and K. Domen, *Microporous Mater.*, **9**, 253 (1997).

9 M. Kohno, S. Ogura, K. Sato, and Y. Inoue, *J. Chem. Soc., Faraday Trans.*, **93**, 2433 (1997).

10 S. Tabata, H. Ohnishi, E. Yagasaki, M. Ippommatsu, and K. Domen, *Catal. Lett.*, **28**, 417 (1994).

11 S. Ikeda, M. Hara, J. N. Kondo, K. Domen, H. Takahashi, T. Okubo, and M. Kakihana, *Chem. Mater.*, **10**, 72 (1998).

12 M. P. Pechini, U. S. Patent 330697 (July 1967).

13 H. Kato and A. Kudo, *Catal. Lett.*, **58**, 153 (1999).

14 H. Kato and K. Kudo, *Chem. Lett.*, **1999**, 1027.

15 H. Kato and A. Kudo, *Chem. Phys. Lett.*, **295**, 487 (1998).

16 A. Kudo, H. Kato, and S. Nakagawa, *J. Phys. Chem. B*, in press.

17 A. Kudo and H. Kato, *Chem. Lett.*, **1997**, 867.

18 T. Ishihara, H. Nishiguchi, K. Fukamachi, and Y. Takita, *J. Phys. Chem. B*, **103**, 1 (1999).

19 M. P. Dare-Edwards, J. B. Goodenough, A. Hamnett, and N. D. Nicholson, *J. Chem. Soc., Faraday Trans. 2*, **77**, 643 (1981).

20 N. Serpone and E. Pelizzetti, "Photocatalysis," Wiley, New York (1989), and references therein.

21 A. Kudo and M. Sekizawa, *Catal. Lett.*, **58**, 241 (1999).

22 A. Kudo, K. Ueda, H. Kato, and I. Mikami, *Catal. Lett.*, **53**, 229 (1998).

23 A. Kudo, K. Omori, and H. Kato, *J. Am. Chem. Soc.*, in press.

24 J. Yoshimura, Y. Ebina, J. Kondo, and K. Domen, *J. Phys. Chem.*, **97**, 1970 (1993).

25 Y. Inoue, Y. Asai, and K. Sato, *J. Chem. Soc., Faraday Trans.*, **90**, 797 (1991).

26 M. Kohno, S. Ogura, and Y. Inoue, *J. Mater. Chem.*, **6**, 1921 (1996).

27 Y. Inoue, T. Kubokawa, and K. Sato, *J. Chem. Soc., Chem. Commun.*, **1990**, 1298.

28 Y. Inoue, T. Kubokawa, and K. Sato, *J. Phys. Chem.*, **95**, 4059 (1991).

29 Y. Inoue, T. Niiyama, and K. Sato, *Top. Catal.*, **1**, 137 (1994).

30 S. Ogura, M. Kohno, K. Sato, and Y. Inoue, *J. Mater. Chem.*, **8**, 2335 (1998).

31 M. Kohno, S. Ogura, K. Sato, and Y. Inoue, *Stud. Surf. Sci. Catal.*, **101**, 143 (1996).

32 S. Ogura, M. Kohno, K. Sato, and Y. Inoue, *Phys. Chem. Chem. Phys.*, **1**, 179 (1999).

33 S. Ogura, M. Kohno, K. Sato, and Y. Inoue, *Appl. Surf. Sci.*, **121/122**, 521 (1997).

34 M. Kohno, T. Kaneko, S. Ogura, K. Sato, and Y. Inoue, *J. Chem. Soc., Faraday Trans.*, **94**, 89 (1998).

35 M. Kohno, S. Ogura, K. Sato, and Y. Inoue, *Chem. Phys. Lett.*, **267**, 72 (1997).

36 M. Hara, T. Kondo, M. Komoda, S. Ikeda, K. Shinohara, A. Tanaka, J. N. Kondo, and K. Domen, *Chem. Commun.*, **1998**, 357.

37 S. Ikeda, T. Takata, T. Kondo, G. Hitoki, M. Hara, J. N. Kondo, K. Domen, H. Hosono, H. Kawazoe, and A. Tanaka, *Chem. Commun.*, **1998**, 2185.

38 S. Ikeda, A. Tanaka, H. Hosono, H. Kawazoe, M. Hara, J. N. Kondo, and K. Domen, *Stud. Surf. Sci. Catal.*, **121**, 301 (1999).

39 S. Ikeda, T. Takata, M. Komoda, A. Tanaka, H. Hosono, H. Kawazoe, M. Hara, J. N. Kondo, and K. Domen, *Phys. Chem. Chem. Phys.*, **1**, 4485 (1999).

40 M. Hara, H. Hasei, M Yashima, S. Ikeda, T. Takata, J. N. Kondo, and K. Domen, *Appl. Catal. A*, **190**, 35 (1999).

41 M. Hara, M. Komoda, H. Hasei, M. Yashima, S. Ikeda, T. Takata, J. N. Kondo, and K. Domen, *J. Phys. Chem. B*, **104**, 780 (2000).

42 R. D. Shannon, D. B. Rogers, and C. T. Prewitt, *Inorg. Chem.*, **10**, 713 (1971).

43 C. T. Prewitt, R. D. Shannon, and D. B. Rogers, *Inorg. Chem.*, **10**, 719 (1971).

44 S. Ikeda, Ph. D Thesis, Tokyo Institute of Technology (1999).

45 T. Uchijima, M. Takahashi, and Y. Yoneda, *Bull. Chem. Soc. Jpn.*, **40**, 2767 (1967).

46 P. G. Gravelle, G. El. Shobaky, and H. Urbain, *Compt. Rend.*, **262**, 549 (1966).

47 M. C. Shaw, *J. Appl. Mechanics*, **15**, 37 (1948).

48 S. Mori, T. Kawada, and W.-C. Xu, *Appl. Surf. Sci.*, **108**, 391 (1997).

Prof. Kazunari Domen was born in 1953 in Kagoshima. He was graduated from the University of Tokyo in 1976 and finished doctor course there in 1982. He joined Tokyo Institute of Technology in 1982 as associate researcher. He was promoted to associate professor in 1990. He was promoted to professor in 1996. He obtained Ph.D. degree from the University of Tokyo in 1982. His research interests include physical chemistry, and chemical reaction dynamics heterogeneous catalysis and photocatalysis.

Dr. Junko N. Kondo was born in 1963 in Kanagawa. She was graduated from the Science University of Tokyo in 1986 and finished doctor course Tokyo Institute of Technology in 1991. She joined Tokyo Institute of Technology in 1991 as associate researcher. She obtained Ph.D. degree from the University of Tokyo Institute of Technology in 1991. Her research interests include catalysis and material science.

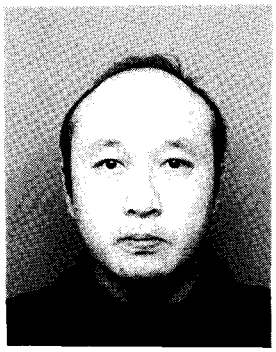

Dr. Michikazu Hara was born in 1965 in Tokyo. He was graduated from the Science University of Tokyo in 1987 and finished doctor course Tokyo Institute of Technology in 1992. After 3 years work in Japan Toshiba as a researcher, he joined Tokyo Institute of Technology in 1995 as associate researcher. He obtained Ph.D. degree from the University of Tokyo Institute of Technology in 1992. His research interests include chemistry, and electro- and photochemistry and catalysis.

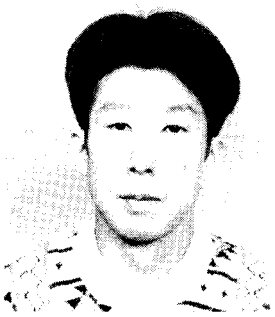

Mr. Tsuyoshi Takata was born in 1971 in Hyogo. He was graduated from the University of Waseda in 1995 and belong to doctor course Tokyo Institute of Technology now. His research interests include photocatalysis and inorganic synthesis.